UNIVERSITEIT VAN PRETORIA
UNIVERSITY OF PRETORIA
YUNIBESITHI YA PRETORIA

Faculty of Engineering, Built Environment and Information Technology

Modelling and multi-objective optimisation of heat transfer characteristics and pressure drop of nanofluids in microtubes

Mr M Meyer

14011809

Supervisor: Dr Mehdi Mehrabi

Co-supervisor: Prof Josua P Meyer

2020-02-11

Department of Mechanical and Aeronautical Engineering

ABSTRACT

Author: Marcel Meyer (u14011809)

Supervisor: Dr Mehdi Mehrabi

Co-supervisor: Prof Josua P Meyer

Department: Mechanical and Aeronautical Engineering

University: University of Pretoria

Year: 2019

A literature study was performed on the inner mechanisms of nanofluids and flow in microchannels. With ever changing technology, the need for smaller and more efficient devices has come about in the last couple of years. With the shrinking in size of components in electronics, an increase in heat has become a notable problem. With conventional heat transfer fluids not being able to handle the required heat removal rates, research into fluid enhancing has been of great interest. A nanofluid is a fluid with enhanced heat transfer potential, which can solve the problem of extracting enough of the added heat of new-age components. This will allow electronics to work with increased power and accomplish tasks faster. Nanofluids have been a very controversial method of heat transfer as problems with stability were keeping the fluid from replacing traditional heat transfer fluids.

Some research has been done on the models used for simulating and defining the thermal properties of nanofluids. Added accuracy of the models has been seen in recent years. However, no optimal setup for nanofluids has been found in terms of combining parameters like the base fluid and nanoparticle, as well as the concentration and diameter of the nanoparticle. An optimal setup of this kind would produce the best heat transfer rates at the lowest pressure drop. The simulation of nanofluids was done in Ansys CFD. The validation was done with previous literature that had experimental and numerical results. The validation had a very good outcome as some of the temperature data inside the microchannel presented a good correlation to previous work. The setup of the model for simulation and duplication to create a design study was also described and shown. This was done to ensure that the model can be used again if further investigation is needed. This will enable one to determine the effect of a new nanoparticle on the field of study to continuously improve on the model.

The results indicated the best nanoparticle to use with the best base fluid to ensure the lowest pressure drop and highest heat transfer. This was done with a multi-objective optimisation general algorithm. The outcome of the optimisation was that silicon dioxide, as nanoparticle, and water, as base fluid, would give the optimal setup. The diameter also appeared to have a very small effect on the outcome.

CONTENTS

LIST OF FIGURES

LIST OF TABLES

NOMENCLATURE

A	Cross-section area
c_p	Specific heat capacity (J/kgK)
C1	Dissipation Rate constant
C2	Dissipation Rate constant
D_h	Hydraulic diameter(4A/P)
d_p	Diameter of nanoparticle
E_{ij}	Rate of Deformation
F	Pressure drop coefficient
H_{ch}	Depth of microchannel
H_{hs}	Depth of heat sink
h	Heat transfer coefficient(W/m2K)
k	Fluid thermal conductivity (W/mK)
k_s	Solid thermal conductivity (W/mK)
L_{ch}	Length of microchannel (m)
$\dot{m}$	Mass flow rate (kg/sec)
M	Molecular weight (g/mol)
N	Avogadro Constant
P	Wetted perimeter (m)
p	Pressure (Pa)
$\dot{q}_w$	Heat flux at base plate (W/m2)
$\dot{Q}$	Fluid flow rate (m3/s)
Re	Reynolds Number
s	Radial Basis Function general form
T	Temperature (K)

T_{hs}	Mean Temperature (K)
T_{ave}	Mean fluid Temperature (K)
T_b	Fluid bulk Temperature (K)
u	Velocity in x direction (m/s)
u_i	Velocity in x Direction (m/s)
v	Fluid velocity in the y direction (m/s)
V	Velocity (m/s)
w	Fluid velocity in the z direction (m/s)
x_i	In the X-axis direction
x,y, z	Coordinate system

Greek symbols

ρ	Density (kg/m3)
ϕ	Volume fraction (%)
μ	Dynamic viscosity (Ns/m2)
μ_t	Eddy Viscosity (Ns/m2)
∇	Partial derivative in respect to direction
∂	Partial Derivative
σ_k	Strain Rate
ε	Rate of dissipation
ζ	data sites
λ_ζ	Radial Basis Function coefficients
$\varphi(r)$	Radial Basis Function

Subscripts

ch	Channel

h	Hight
p	Particle
hs	Heat Sink
s	Solid
w	Heat flux
ave	Average
b	Bulk
i	Mathematical place holder used in case of expansion of equations
t	Time (s)

Operators

$\vec{}$	Direction Vector
·	Dot Product
‖ ‖	Euclidean distance

Abbreviations

GCI	Grid Convergence Index
UDF	User defined function
MCHS	Microchannel heat sink

CHAPTER 1: INTRODUCTION

1.1 BACKGROUND

Energy demands in a constantly growing society have become more challenging and burdensome on the environment. As a result, the development of sustainable green energy has been increasing over the last couple of years. The growing population adds strain on the planet and resources are being stretched thin. The initiative to produce more energy with lower cost and negative impacts on the planet are on the rise.

With evolving technology, electrical and mechanical systems are becoming smaller and more efficient. This often leads to increased heat flux generation (heat per unit area). The removal of this excess heat has become a new focus point of research and development. If a component is allowed to overheat, performance reduction can be severe. Equipment damage and hot spots decrease efficiency. Therefore, an increase in the earth's population results in advancements in technology that are driven by the need for faster and more efficient systems, which require enhanced cooling mechanisms.

Thermal management has a couple of solutions. One of the most-used methods, is altering the geometry by adding fins and functional material. This increases the effective heat transfer surface of microchannels, increasing the heat transfer coefficient and lowering temperatures. This, however, also increases the production costs as the geometry can turn out to be very complicated and advanced. Microchannels' very low fluid volume does not allow heat transfer to be as efficient as required. Microchannels are used because of the smaller components and thus another fluid has to be used to obtain the required heat removal.

The modification of the heat transfer fluid is a new method that is currently possible due to the increased technology of nanofluid preparation. A nanofluid is made by dispersing very small particles and a working base fluid to increase the heat transfer coefficient. The idea of creating a fluid with the properties of a metal is a concept that is strived for. The thermal conductivity of metal is much higher than that of fluid. Therefore, the addition of nanoparticles, which consist of metal, to a fluid, would increase the overall thermal conductivity, decrease the pumping power required and increase the thermal efficiency required. The different particles that can be used are metal, metal oxide, non-metals dispersed inside water, ethylene glycol (EG), glycerol, propylene glycol (PG) or engine oil. This dispersion will change the heat transfer properties of the liquid. Therefore, nanofluids will be a big benefit to any system that has a working fluid, especially heat transfer systems.

1.2 AIM OF THIS RESEARCH

The aim of this research is to model a nanofluid flow field in a microchannel in order to analyse and optimise heat transfer characteristics and pressure drop. This is done by using set material property models for nanofluids and inspecting the effect of changes in the base fluid, nanoparticle type, particle diameter and particle concentration. Setting up such a model will allow the researcher to analyse any combination of inputs in a design study. The model created will ensure that further research into the field of nanofluids can be done faster and more efficiently.

1.3 RESEARCH OBJECTIVES

This study has the following research objectives:

- Perform an in-depth literature study about the working mechanisms of nanofluids.
- Characterise different nanofluids with Ansys Fluent software.
- Validate the results against a numerical study obtained from the literature.
- Develop a model for creating a design study that is solved using Ansys Fluent, which is capable of analysing the effect of different nanofluids on pressure drop and heat transfer.
- Perform the multi-objective optimisation and characterisation of the design study data.

1.4 SCOPE OF THIS STUDY

The scope of the study is to investigate the influence of nanoparticle size, volume fraction, base liquid and type on pressure drop and heat transfer properties. The selection of nanoparticles will be chosen to compare and validate results from literature. In-house optimisation codes will be used in conjunction with genetic algorithms and neural networks to optimise the input parameters for pressure drop to be at a minimum and heat transfer to be at a maximum.

The models for characterising the nanofluids will not be built from scratch as an existing model will be used and implemented. The focus of the project is to optimise the material property inputs of Ansys Fluent and build a model that will enable repeatability. For instance, if a new nanoparticle is developed, the properties can be added to the model and a design study can be created automatically and solved. The optimisation code can then be run to determine what new influence the nanoparticle has on the field of study.

1.5 PROBLEM STATEMENT

Models for nanofluids have been developed in recent years with increasing accuracy to achieve experimental results. However, with so many models and parameters that can be modified for use with nanofluids, an optimal setup has not yet been found. This study aims to fill the knowledge gap regarding which parameters to use in conjunction with which other parameters to achieve the optimal balance. While some of the literature refers to optimal settings, no cases of using artificial intelligence or machine learning have been established to optimise a wide variety of parameters.. This will allow the user to input different configurations, as well as base fluids, concentration and particle diameter in order to optimise the parameters to achieve the best configuration for heat transfer and pressure drop.

1.6 ORGANISATION OF THE THESIS

Chapter 1 introduces the concept and the use of nanofluids as a new working fluid in heat transfer applications. The reason for the study, as well as the aims and objectives, are clearly detailed. As this is an introductory study that will be used as the foundation for future work, the scope is also defined.

Chapter 2 presents a summary of the theory and concepts that need to be understood and used to correctly implement a nanofluid in a numerical simulation. A detailed account of the preparation, stability and properties that influence nanofluids is given. Optimisation as a concept and tool is added for future work.

Chapter 3 discusses the methodology used to set up a model to ensure that the next user of the model knows how to operate and continue using it.

Chapter 4 describes the validation of the numerical study from data obtained in literature. It also discusses the creation of the design study and the parameters that were changed, as well as how the parameters were combined to ensure that enough data is generated for optimisation. This section also describes the characterisation of the design study data and its optimisation.

CHAPTER 2: LITERATURE REVIEW

2.1 INTRODUCTION

The study of suspension and dispersion can be traced back to Maxwell (1873). It was originally his idea to create a fluid with enhanced properties. At the time, technology was not sufficiently advanced to make particles fine enough for full dispersion, and the settlement of particles occurred. Recent studies show that the creation of particles as small as 10 nm can possibly solve the problem of stagnation and increase stability. It has been shown that the new method of cooling components in either electrical or mechanical systems can be achieved with higher efficiency with nanofluids than with traditional heat transfer fluids. Forced convection through microchannels can then provide a cooling solution for microelectromechanical components used in computers, as these components run at high temperatures, even with water cooling. Simulations of nanofluids have been a new focus for research to test the capabilities of the new working fluids. These simulations have been confirmed as not being that complicated if the correct properties are implemented.

The introduction of new-age nanofluids may be accredited to Choi (1995). Based on the studies of Maxwell (1873), nanoparticles were suspended in a base fluid. Nanofluids are thus colloidal suspensions that contain nanoparticles, which can range from 10 to 100 nm in size (Buschmann et al., 2018).

The following particles have been identified:

- Metallic (Ag, Au, Al, Cu and Ni)
- Non-metallic (graphene, graphite)
- Metal oxide (CuO, SnO_2, MgO, Fe_2O_3)
- Multi elements
- Carbides and non-metals

Nanofluids are suspended in normal household fluids such as water, engine oil, transformer oil or a mixture of heat transfer fluids. The first fluids with colloidal suspensions were prone to abrasion and the clogging of flow paths. The settlement of the particles would decrease the flow efficiency. Their use was thus not advisable in engineering applications. New nanofluids with much smaller particle sizes require less pumping power and no clogging has yet been reported. Although the methodology of employing such fluids has become quite sophisticated, it still requires further honing before it can be used to its full advantage. The stability of nanofluids, for instance, can still be a problem.

Some of the preparation methods will be discussed in Chapter 2.3.

The classification of nanofluids has been a very open topic and a plethora of models and different equations exist. Each of the subsequent models has been used and verified with different scenarios and models. Some models have been tested and verified more than others. The challenge is to find the correct model for the geometry. Further investigation will be performed later in this chapter. The focus of this report will be the implementation of an Ansys model that has been verified and tested. This will allow for the optimisation of input parameters.

2.2 PREPARATION METHODS FOR NANOFLUIDS

Nanofluids need preparation to ensure that the particles are dispersed evenly in the base fluid to prevent the stagnation or agglomeration of particles. This will improve effectiveness and ensure that the enhanced properties of the nanofluids are indeed retained. The preparation of nanofluids requires two processes: the preparation of dry nanoparticles and their dispersion into the base fluids. Preparation methods are mainly done with physical and chemical procedures.

- Physical
  - Pulsed laser ablation
  - Laser deposition
  - Matrix-assisted pulsed laser evaporation
  - Ball milling
- Chemical
  - Chemical precipitation
  - Sonoelectrochemical synthesis
  - Spray pyrolysis
  - Chemical vapour deposition
  - Thermal decomposition

2.2.1 One-step method

To ensure that the nanoparticles do not agglomerate or stagnate, a one-step method is applied. The method, which utilises vapour condensation, was developed by Eastman et al. (2001). With this method, particles are made and dispersed at the same time. The process aims to simplify the preparation to exclude drying, transportation and storage. This minimises agglomeration and increases the stability of the particles and the fluid. Another one-step method is the vacuum submerged arc nanoparticle synthesis system (SANSS). This method uses some dielectric fluids for the procedure (Eastman et al., 2001). The particles that have been prepared have some of the following shapes: circular, tubular and polygonal.

The method works reasonably well and seems to prevent particle agglomeration. However, it is only suitable for small-scale projects as it cannot be used with large volumes of base liquid. Another one-step method is now being developed and implemented. The chemical method requires the preparation of copper oxide nanofluids by reducing the $CuSO_4$ H_2O with NaH_2PO_2 under microwave irradiation (Mukherjee, S. (2013)) This method can also be used with silver-based nanofluids, which have to be stabilised with Korantin corrosion inhibitor. A dense layer is formed around the particles, keeping them from stagnating. The silver particles remain stabilised for one month. One of the biggest pitfalls of one-step methods is the residuals left inside the fluid. This is as a result of an incomplete reaction.

2.2.2 Two-step method

This method is widely used to prepare nanofluids. The particles are produced as dry powders by any chemical or physical method. The top-down approach is where the particles are produced by crushing larger matter, whereas the bottom-up approach produces nanomaterials from smaller matter. The powder is then released into the fluid and agitated using one of the following methods.

- Magnetic force agitation
- Ultrasonic agitation
- High shear mixing
- Ball milling

This method has already been scaled for commercial use and can be used in the preparation of many samples. These samples, however, generally have large surface areas and suffer from aggregation and clogging. A solution to these problems may be found in the use of surfactants, which are used in high-temperature environments. However, this is still being researched, and the stability of the method has not been proven.

2.3 THE STABILITY OF NANOFLUIDS

The agglomeration (clustering) of nanoparticles is a big problem as it decreases the effectiveness of the fluid in terms of heat transfer and leads to clogged microchannels. It is important to consider the stability of nanofluids when preparing them or maintaining a microchannel. The factors that influence dispersion also have to be studied carefully. Methods of establishing increased stability are discussed below.

2.3.1 Stability evaluation

Characterization of a nanofluids stability in accordance with the dispersion quality of the particles is crucial for the active research of dispersion techniques. Zeta potential was introduced as the first step

in analysing the dispersion stability. Zeta potential is the electric potential between the base fluid and the fluid layer that has attached to the nanoparticles. High Zeta potentials form stable dispersed nanofluids and low Zeta potentials offer nanofluids that aggregate more easily. A value of 30mV or higher is seen as a stabilized fluid (Yu et al.)

Sedimentation and centrifugation methods

The simplest method of stabilising nanofluids has to be sedimentation. The weight or sediment volume of the particles is an indication of the stability of the fluid.

Equipment is available to track variations in concentration (Davis, 1942). Stability is reached when the concentration of the supernatant particles remains constant in solution. A photograph showing nanofluids in a clear tube also indicates stability. When any sedimentation is observed at the bottom of the tube, it indicates that stability has been degrading. It takes a long time to evaluate sedimentation, though, as the specimen has to be studied in detail (Mukherjee, S. (2013)) .(Singh *et al.*, 2016). have developed a new method of stabilisation, the centrifugal method. They found that nanofluids prepared with the PVP stabilisation agent remain stable for more than a month, and for just under 10 hours using centrifugation (Kamatchi and Venkatachalapathy, 2015).

Dispersion methods

Once the nanofluids have been prepared and their stability evaluated, stabilisation mechanisms need to be employed to disperse the particles even further and ensure that stability is improved for long-term use. Two such methods exist: electrostatic and steric stabilisation (Yu et al., 2017). The main objective of these methods is to increase the repulsive interparticle interaction.

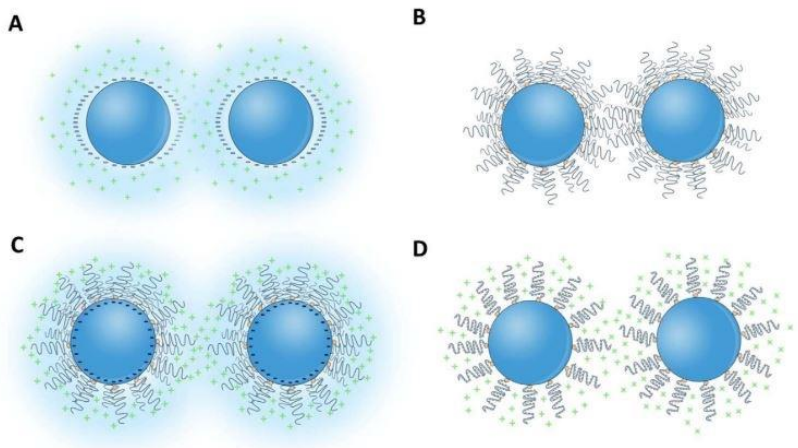

Figure 1: Stabilisation mechanisms

Electrostatic stabilisation is achieved by manipulating the surface charges of the particles, which are formed through absorption, substitution, the accumulation of electrons on the surface and the dissociation of surface charge particles.

The charged particles in the fluid medium will be surrounded by an equal number of counter-ions to ensure charge neutrality in the medium. This will cause a double electrical layer (Brinker, 1990). This double layer causes repulsion between the particles and improves stability (as can be seen in Figure 1).

The DLVO model (named after Derjaguin, Landau, Verwey and Overbeek) explains this stabilisation theory as the interaction between particles, which is attributed to a combination of Van der Waals attraction and electrostatic repulsion. Electrostatic repulsion is only viable in a medium with no electrolytes. However, as electrolytes reduce the repulsion potential, they also disturb the stability and cause an aggregation of particles. The only medium that is suitable for electrostatic repulsion is therefore a dilute nanoparticle dispersion within a polar medium such as water and ethanol. Once the electrostatic stabilisation is broken, the dispersion of particles is no longer possible. (Yu et al., 2017)

Steric stabilisation, on the other hand, causes polymer chains to attach to the nanoparticles and act as a steric barrier between them. This cancels the inter-particle attraction of the Van der Waals forces(Patel and Russel, 1989). This polymer can be irreversibly bound to the particles. Steric stabilisation has the following advantages over electronic stabilisation:

- It can be applied to more fluids and particles.
- High concentrations of nanoparticles can be redispersed.
- The deseparation can happen in an electrolyte fluid as well.
- Different particles can be dispersed in the same base fluid.

Under certain conditions, it is possible to combine the two methods of electrostatic and steric stabilisation (see Figure 1c and 1d). This will form a combined prevention of agglomeration. However, some of the disadvantages of electrostatic stabilisation will still be retained.

2.4 PROPERTIES

Following the preparation of the nanofluids, the evaluation of their stability and a discussion of dispersion methods, Ansys Fluent software is used to simulate different nanofluids. Their thermal properties give them an advantage over normal heat transfer fluids. The effectiveness of the single-phase heat transfer simulation of a Newtonian fluid will depend on the correct implementation of the thermophysical properties in modelling (Buschmann et al., 2018). The classification of nanofluids will

be discussed below. As there are so many models, however, only the most used models will be discussed.

The models that will be used will depend on the verification literature that is used to compare them. In recent studies, higher thermophysical properties of nanofluids have been shown. This indicates that higher heat transfer rates can be achieved and thus utilised in the modern technology environment. The result of these studies confirms that nanofluids can be modelled with Newtonian single-phase heat transfer liquids if the correct properties of the fluid are utilised (Buschmann et al., 2018). Maxwell (1873) used the effective medium theory (EMT) to estimate the transport properties of homogeneous systems.

Using second-order expansion in EMT, certain base equations can be derived, as is shown in Chapter 2.4.1. The values for thermal conductivity, density and specific heat capacity in this study were predominantly sourced from Mirzaei and Dehghan (2013), Azizi, Alamdari and Malayeri (2015), Abdollahi et al. (2017) and Bowers et al. (2018).

Mechanisms of nanofluids

To understand the thermal conductivity of nanofluids, it is important to examine their particle size, shape and volume fraction. If one assumes that diffusive heat transfer takes place in the solid and the fluid, modelling can be attempted using only these parameters. It has been found that this method has a very good correlation with two-phase systems with larger particles (in the micrometre range). However, it fails to completely define the characteristics of nanofluid heat transfer. Two categories can be used to foster an understanding of thermal transport properties. The first describes thermal conductivity in terms of the fluid's conventional static part, coupled with an added Brownian motion. The Brownian motion presents a micro-mixing feature to the nanofluids. Models of this kind include particle dynamics, as well as fluid dynamics, thus the particle size, thermal conductivity and volume fraction and temperature of both phases are used.

The second category approaches the properties from the side of the nanostructure, assuming that it consists of a core and a shell immersed in a fluid. It is therefore a three-phase medium theory for a multiphase system, which argues that the enhanced thermal properties come from the ordered layer of fluid particles around the nanoparticles. However, the precise methods and mechanisms are not known and are still being researched. A number of researchers have reported advances in thermal conductivity theory. Some explanations for increased thermal conductivity will be detailed below, but it needs to be understood that each theory, model and equation presented has its advantages and disadvantages.

Eastman (2004) and Keblinski (2002) studied the motion molecular layering of nanoparticles, heat transport, nature and particle clustering. They found that Brownian motion could be neglected as it had no foreseeable effect on thermal conductivity. However, they only studied stationary fluids. Wang (1999) expressed the opinion that the microscopic motion caused by Brownian and other inter-particle forces explains the increased effects. (Xuan and Li, 2000) added that the effects could be from the increased surface area added by the particles. The concept of interfacial layers between the particles has recently been explored by a few researchers. Choi (2003) has been using models based on liquid molecular layers around the particles. This was disputed by Xue et al. (2004), who noticed that simple monatomic liquids had no effect on heat transfer properties. Thus, thermal transport cannot be perfectly defined by a liquid layer.

No perfect model exists for the improved behaviour of nanofluids, but continuing research activity over recent years is approaching a solution.

2.4.1 Thermal conductivity

With such a variety of models being used, each validated for different cases and geometries, the selection of a model for thermal conductivity is still a disputed one. Some models are used for specific boundary conditions, and thus validation has to be done with experimental results to ensure the usability of a model. Most of the models are based on the following equation for a two-phase mixture:

$$k_{eff} = \frac{k_{np}\phi_{np}\left(\frac{dT}{dx}\right)_{np} + k_f\phi_f\left(\frac{dT}{dx}\right)_f}{\phi_f\left(\frac{dT}{dx}\right)_{np} + \phi_f\left(\frac{dT}{dx}\right)_f} \quad (1)$$

Maxwell (1873) was one of the first researchers to implement the equation of bigger particles using the following equation:

$$k_{static} = k_f\left[\frac{\left(k_{np} + 2k_f\right) - 2\phi\left(k_f - k_{np}\right)}{\left(k_{np} + 2k_f\right) + \phi\left(k_f - k_{np}\right)}\right] \quad (2)$$

where k_f is the thermal conductivity of the fluid, k_{np} is the thermal conductivity of the nanoparticle and phi is the volume fraction of the suspended nanoparticle.

(Tjaden *et al.*, 2016)has proposed a model ensuring that the interactions between particles are utilised. For spherical inclusions, the following equation is given:

$$\phi\left(\frac{k_{np} - k_{eff}}{k_{np} + 2k_{eff}}\right) + (1 - \phi)\left(\frac{k_f - k_{eff}}{k_f + 2k_{eff}}\right) = 0 \quad (3)$$

From the model in Equation 1, no limitations on concentration are present. For very small solid concentrations, this model gives almost the same answers as the model of Maxwell (1873). The model Bruggeman (1935) has been compared to the experimental data of Choi (1995), and performed well.

For the inclusion of non-spherical particles, Hamilton and Crosser (1962) developed a model with an included shape factor, as detailed in Equation 3

$$k_{eff} = \frac{k_{np} + (n-1)k_b - (n-1)\left(k_f - k_{np}\right)\phi}{k_{np} + (n-1)k_{nb} + \left(k_f - k_{np}\right)\phi} \tag{4}$$

where n is defined as $n = \frac{3}{\varphi}$, a shape factor dependent on the sphericity of the used particle.

This model correlates with that of Maxwell (1873) for $n = 1$. If a sphericity of 1 is added, Maxwell's model is achieved. Newer models have been more focused on the effects of clustering particles and nanolayers between particles.

Yu (2003) developed a model accounting for nanolayers by substituting k_p with a modified thermal conductivity of k_{pe}.

$$k_{pe} = \frac{(2(1-\gamma) + (1+\beta)^3(1+2\gamma)\gamma}{-(1-\gamma) + (1+\beta)^3(1+2\gamma)} \tag{5}$$

where gamma is defined as $\gamma = \frac{k_{layer}}{k_p}$ and beta is the ratio of nanolayer thickness to the original particle thickness, $\beta = \frac{h}{r}$. Thus, the following equation is derived from Maxwell's original model:

$$k_{eff} = \frac{k_{pc} + 2k_f + 2\left(k_{pc} - k_f\right)(1-\beta)^3\phi}{k_{pe} + 2k_f - \left(k_{pe} - k_b\right)(1-\beta)^3\phi} k_b \tag{6}$$

This model concluded that reducing the diameter of the nanoparticle and the thickness of the nanolayer, thermal conductivity can be improved. Yu (2003) then decided that adding non-spherical particles to the already resolved nanolayer would deliver a better model, and in 2004 developed a new model based on the model of Hamilton and Crosser (1962) in Equation 7

$$k_{eff} = \left(1 + \frac{b\phi A}{1 - \phi A}\right) k_b \tag{7}$$

where A is used as $A = \frac{1}{3}\sum_{j=a,b,c} \frac{k_{pj} - k_b}{k_{pj} + (n-1)k_b}$ and $\phi = \frac{\phi_1 \sqrt{(a^2+t)(b^2+t)(C^2+t)}}{\sqrt{abc}}$

This model describes carbon nanotubes in an oil base, but fails to describe the general metal- and oxide-based nanofluids. This reiterates the fact that the models are developed such specific cases and the choice of a model is critical before implementation can start.

Xue (2003) designed a model incorporating the polarisation effect induced by the fluid on the particles. In Equation8, it can be displayed as follows:

$$9\left(1-\frac{\phi}{\lambda}\right)\frac{k_{eff}-k_b}{2k_{eff}+k_b}+\frac{\phi}{\lambda}\left(\begin{array}{c}\frac{k_{eff}-k_{cx}}{k_{eff}+B_{2x}\left(k_{cx}-k_{eff}\right)}+\\ \frac{4\left(k_{eff}-k_{cy}\right)}{2k_{eff}+(1-B_{2x})\left(l_{cy}-k_{eff}\right)}\end{array}\right)=0 \tag{8}$$

This model is fairly complex and hard to implement. The constants that need to be calculated were even implemented incorrectly by Xue himself, so that he found unsatisfactory results in testing the equation against the experimental results of Xue and Xu (2005).

In recent studies, the temperature dependence of thermal conductivity has been more deeply investigated. Xuan (2003) considered Brownian motion derived from Maxwell's equations and modified the equation.

$$k_{eff}=\frac{k_{np}+2k_f-2\left(k_f-k_{np}\right)\phi}{k_{np}+2k_f+\left(k_f-k_{np}\right)\phi}k_b+\frac{\rho_p\phi c_p}{2}\sqrt{\frac{k_BT}{3\pi r_c\mu}} \tag{9}$$

where $k_B=1.381x10^{-23}J/K$ is the Boltzmann constant.

This model incorporates the temperature dependence, but according to the experimental data of Das (2003), the dependence was not strong enough at $\propto T^{0.5}$.

More recently, Koo and Kleinstreurer (2004) introduced a model that incorporates Brownian motion, particle size, particle volume and temperature dependence. The formula results in:

$$k_{eff}=\frac{k_{np}+2k_f+2\left(k_{np}-k_f\right)\phi}{k_{np}+2k_f-\left(k_{np}-k_f\right)\phi}k_f+5\times10^4\beta\phi\rho_pc_p\sqrt{\frac{k_BT}{\rho_pD}}f(T,\phi) \tag{10}$$

with the temperature dependence function is as follows:

$f(T,\phi)=(-6.04\phi+0.4705)T+(1.722.3\phi-134.63)$.

The equations shown above, viewed against the specific considerations of each model, explain the earlier comment that modelling equations and parameters depend on the verification literature

against which results are to be compared. Models are developed for such specific cases, which means that the choice of model is critical.

2.4.2 Specific heat capacity

The implementation of specific heat capacity and density has been proven to be very simple and straightforward, as explained above. The following equations are more popular and are used throughout:

$$C_{pnf} = \frac{(1-\varphi)(\rho C_p)_f + \varphi(\rho C_p)_s}{\rho_{nf}} \tag{11}$$

2.4.3 Density

$$\rho_{nf} = (1-\varphi)\rho_f + \varphi\rho_s \tag{12}$$

2.4.4 Viscosity

The first model for the viscosity of the suspension of spheres in a base fluid was developed by Einstein in 1956, using hydrodynamic equations. He derived the following equation:

$$\mu_{eff} = (1 + 2.5\phi_p)\mu_b \tag{13}$$

The assumption Einstein originally made was that the disturbance of the fluid by a particle does not intersect with the disturbance of a second suspended particle. A wide variety of models has been developed since the 1950s. However, these models all pre-date nanofluids and cannot precisely predict their behaviour. Newer models consider nanofluid research and more focus will be added to these models (Adio, 2015).

Masoumi et al. (2009) developed a model based on Brownian motion, which incorporated five parameters: temperature, size, concentration, density and fluid properties. The validation of this model was done with two-phase and single-phase cases. This can be seen in Equation14.

$$\mu_{nf} = \mu_o + \frac{\rho_p V_B d_p^2}{72C\delta} \tag{14}$$

with delta being defined as $\delta = \sqrt[3]{\frac{\pi}{6\phi}}d_p$

The following model, designed by Hosseini et al. (2010), was developed with the idea of dimensionless groups incorporating the volume fraction and the diameter of the particles, as well as the viscosity of

the base fluid and the capping layer as $\pi_{1,2,3,4}$ respectively. The groups and viscosity are shown by the following model equations $\pi_1 = \frac{\mu_{nf}}{\mu_o}\,\pi_2 = \phi_h\,\pi_3 = \frac{d}{1+r}\,\pi_4 = \frac{d}{1+r}\cdot m$

$$\mu_{nf} = \mu_o \cdot \exp\left(m + \alpha\left(\frac{T}{T_o}\right) + \omega(\phi_h) + \gamma\left(\frac{d_p}{1+r}\right)\right) \tag{15}$$

A modification of the model developed by Krieger and Dougherty (1959), which ensured that the effect of stagnation and agglomeration was accounted for, was developed by Chen et al. (2007)

$$\mu_{nf} = \mu_o\left(1 - \frac{\phi_a}{\phi_m}\right)^{n\phi_m} \tag{16}$$

An effective volume fraction is added by ϕ_a, where the radii of the agglomerated particles and primary nanoparticles are added.

Most of the models shown above use non-dimensional numbers and values. However, some of the constants can only be obtained from experimental data. This makes these models extremely costly to implement and use correctly. An appropriate model in this study will encapsulate several parameters of the nanofluid; not just temperature dependency. Particle size, for instance, is crucially important. On the other hand, the use of more complex equations takes more time and effort, is more error prone and takes longer to execute. Some of the following equations have been adapted from Einstein's original adaptation. However, other dependencies have been added.

Koo & Kleinstreurer (2005)

$$\mu_{brownian} = 5 \times 10^4 \beta \rho_f \phi_{np} \sqrt{\frac{k_B T}{2\rho_{np} r_{np}}}\left(\left(-134.63 + 1722.3\phi_{np}\right) + \left(0.4705 - 6.04\phi_p\right)T\right) \tag{17}$$

Graham (1981)

$$\mu_{eff} = \left[1 + 2.5\phi + \frac{4.5}{\left(\frac{s_p}{r_p}\right)\left(\left(2 + \left(\frac{sp}{rp}\right)\right)\left(1 + \left(\frac{sp}{rp}\right)\right)^2\right)}\right] \tag{18}$$

Conclusion

As shown above, numerous models for simulating nanofluids are available. To select a specific model for simulation, the specific nature of the nanofluid needs to be kept in mind, as certain models only work for certain fluids and geometries. The most important factor to bear in mind is the number of dependencies a model uses to calculate the properties of the nanofluid. The model developed by Koo and Kleinstreurer (2005) was selected for this project. The model equations can incorporate any

nanofluid. Base fluid and nanoparticle properties are considered, as well as Brownian motion and temperature dependency. The study of Koo and Kleinstreurer (2005) considered the increase of heat transfer performance in micro heat sinks, and thus incorporates the microchannel simulations quite well. The addition of particle diameter volume, concentration and temperature dependency, as well as Brownian motion, ensures that this model covers some of the newly found dependencies on the thermophysical effects of the nanofluid. The model is not too complex to implement as all the constants and factors are known or can be obtained through literature. It is very important to keep in mind the optimisation that will be done in future work. The number of optimisable parameters also depends on the model being used. This was a key deciding factor on the model choice.

As specified above, the density and specific heat capacity is calculated through only one model. These properties will be used as in equations 19 and 20. The thermal conductivity model is shown below, as well as the viscosity in equations 27 and 28, respectively.

$$k_{eff} = \frac{k_{np} + 2k_f + 2(k_{np} - k_f)\phi}{k_{np} + 2k_f - (k_{np} - k_f)\phi} k_f + 5 \times 10^4 \beta \phi \rho_p c_p \sqrt{\frac{k_B T}{\rho_p D}} f(T, \phi) \tag{19}$$

$$\mu_{brownian} = 5 \times 10^4 \beta \rho_f \phi_{np} \sqrt{\frac{k_B T}{2\rho_{np} r_{np}}} ((-134.63 + 1722.3\phi_{np}) + (0.4705 - 6.04\phi_p)T) \tag{20}$$

2.5 OPTIMISATION

2.5.1 Introduction

Optimisation has become the focus of nearly all engineering disciplines. Optimisation entails tuning parameters to ensure a more desired outcome than could be achieved with manual tuning. Optimisation uses algorithms to acquire data from outcomes and predict the influence of certain parameters. These parameters are then altered for the best results. In engineering, where every aspect and component of the discipline is becoming more specialised, better inputs and specifications are needed for heightened results. This is done to get all the components to work faster and harder with the same input, reducing power requirements and increasing performance. This can only be done if the correct parameters are optimised in conjunction with one another. As it would take very long to optimise these parameters manually, optimisation algorithms have been developed that can do this automatically. The main optimisation and machine learning methods in use today are neural networks, genetic algorithms and particle swarm optimisation.

These methods can be used in this study to optimise the parameters of nanofluids to ensure that the best models and configurations are used to get the lowest pressure drop and highest heat transfer coefficient. Parameters that can be optimised in the simulation of nanofluids in a microchannel will influence the configuration of the fluid and the models with which the fluid is resolved. With such a wide variety of available models, the optimal one (that is verified with experimental data) can be used in any specific application.

Three methods can be used for prediction and optimisation. The reason for choosing these three methods is due to the researcher's previous experience with these models and algorithms. Each of these methods has been implemented, and a deeper understanding has already been achieved of how they function and perform. Thus, any implementation or usage will be done to a higher standard as the methods and theory are already understood.

2.5.2 Genetic algorithms

The premise of this optimising scheme is that one could theoretically use brute force optimisation to test all possible inputs. This would, however, take extremely long and a better method has to be found. Genetic algorithms (GAs) made their appearance based on evolution theory. In evolution terms, a GA implements "random" inputs and "breeds better children than their fathers and mothers". The best children are kept and made into fathers and mothers again. This way, the best input combination can be found. However, not every combination is tested. Herein lies the best use of computational time. An optimal combination can be found without having to test every possible solution.

Implementation of a genetic algorithm

- Create a random, yet realistic population of inputs
- Calculate the fitness function for each input (this determines the accuracy of the method)
- Breed with the best performing members
- Mutate a member randomly to cover a wider variety of inputs
- Eliminate the worst-performing members
- Repeat these steps through different generations to narrow down the optimal member

CHAPTER 3: METHODOLOGY

3.1 INTRODUCTION

The following section will detail the methodology and procedure used to generate a full design study to obtain the data needed for the optimisation of nanofluids in a microchannel. Each of the decisions made was done with a view to optimisation. From the geometry to the mesh, as well as the material property equations, each has its own effect on the final optimisation.

The software used for the generation of the data was Ansys Fluent; particularly the relationship between Ansys Fluent and its hub, Ansys Workbench. Workbench links the different variables of a project to each other. This makes it possible to have many different simulations all stored in one place. This is precisely what was needed for the creation of a design study that included the four optimisation variables. The optimisation can only be done when enough points of reference are generated on a design space. Thus, it was decided that a full design study would be done on all the variables: the base fluid, the nanoparticle, the diameter of the nanoparticle and the concentration of particles. This required a brute force method, mapping all iterations of every variable against every iteration of every other variable. This meant that every single combination between the four variables would be simulated to determine their impact. Having four variables resulted in a design table of 256 different instances. Every instance was simulated and the data of each simulation was saved for post-processing and analysis This process generated enough data for optimisation.

A detailed description of the methodology is presented below. This is done to develop a thorough understanding of the methods followed to ensure that the same results can be obtained by another researcher following the same methodology, thereby ensuring the validity of the study.

The goals of the model under construction are as follows:

- Setup of numerous different design points for a design study.
- Efficiently solve the problem to ensure minimal time delays.
- Develop an autonomous model where minimal self-input is needed to help with repeatability.

3.2 GEOMETRY

The geometry has a massive effect on the overall effectiveness of heat transfer. The optimisation criterion for this project was to find the lowest pressure drop, while having the biggest Nusselt number (a quantification of heat transfer). To analyse the effect of the material properties on heat transfer, the geometry has to remain constant. A microchannel was selected as the static geometry for this project, as it represents the most relevant geometry for heat transfer in the field. The configuration of microchannels differs from design to design. It was therefore important to choose a design that conforms to previous research and experiments, as validation of the model is of great importance. Without any validation, the methodology of the model is of no use. The model that is being created will accept any nanofluid and/or particle for numerical testing. This ensures that when new nanoparticles are developed, they can be added to enrich the model and keep it relevant and valuable.

A microchannel with a V-type inlet, as used by Abdollahi et al., 2017, was selected. This made validation easy and, as seen in Chein and Chen, 2009, the microchannel design was indeed the best-performing inlet and outlet configuration for heat transfer.

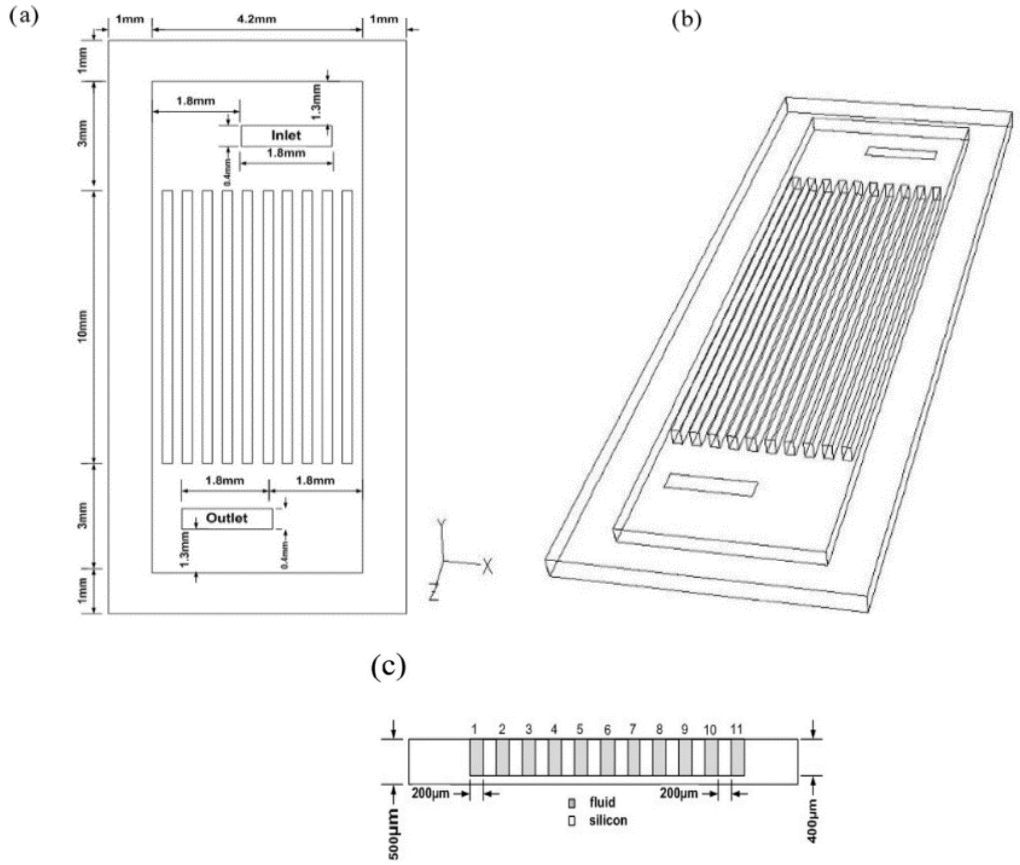

Figure 2: The geometry

The geometry was modelled using SolidWorks Computer-aided Design (CAD) software, but any CAD software will suffice as Ansys accepts most file types. Any geometry can be imported as well. Ansys has a function in the geometry viewer that enables it to correct poor-quality designs to ensure that no gaps are present in the geometry, as this will incur leaks.

The model is very simple to ensure that no complex flow patterns emerge to increase simulation time. As is evident in Figure 2, the flow will enter the channel vertically, hitting an invisible lid and then be forced out through the channels. The main heat transfer will be done through the channels. The outlet is horizontal. The biggest impact that this inlet-outlet arrangement had on the simulation was that some turbulence was created as the fluid swirled around the inlet and the outlet. This caused complications in trying to solve the system in a laminar flow regime, which is the regime prescribed by Ayoub in (Abdollahi et al., 2017).

Laminar flow simplifies equations as turbulence coefficients are assumed to be zero, and drastically reduce computational complexity and time. With no slip assumption at the walls, the perfect flow model would be created inside the channels, but with the inlet swirling, the laminar set of equations could not calculate or define the turbulence at the inlet and outlet. This led to a divergence of the simulations. A steady state of flow could therefore not be achieved.

This was monitored by comparing the temperatures at the outlet and within the channels. In steady state, the temperatures are supposed to stabilise if the simulation has converged. This means that the solution is not changing per iteration and that the global minimum has been achieved. This was not the case when laminar flow was assumed.

Laminar and turbulent flow are shown in Figure 3 and Figure 4, respectively

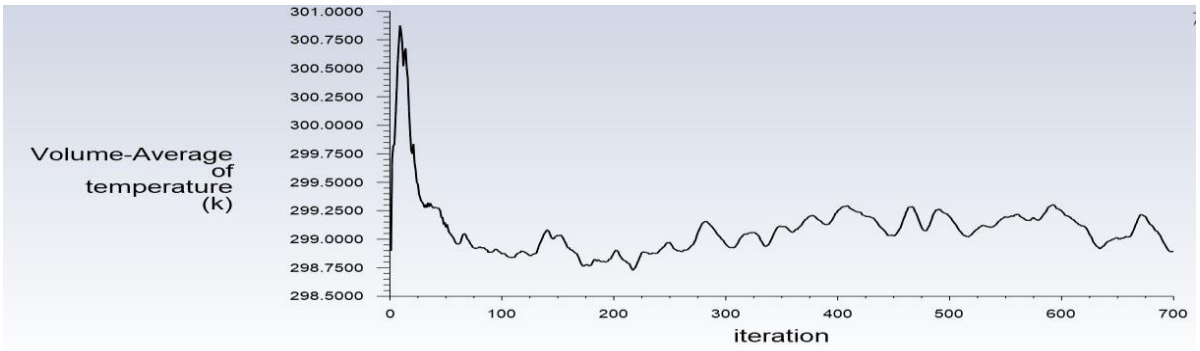

Figure 3: Fluid temperature in the laminar flow regime

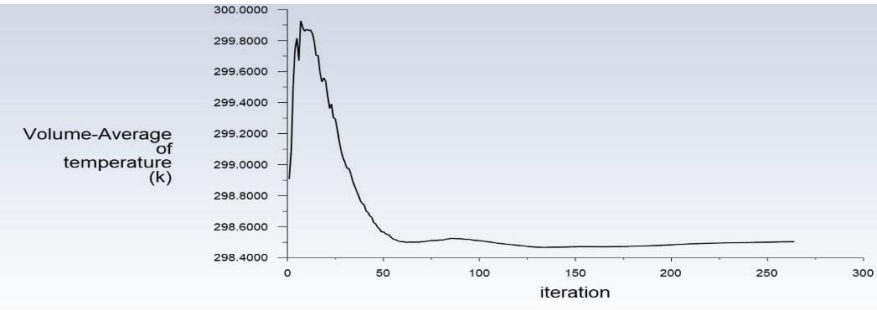

Figure 4: Fluid temperature in the turbulent flow regime

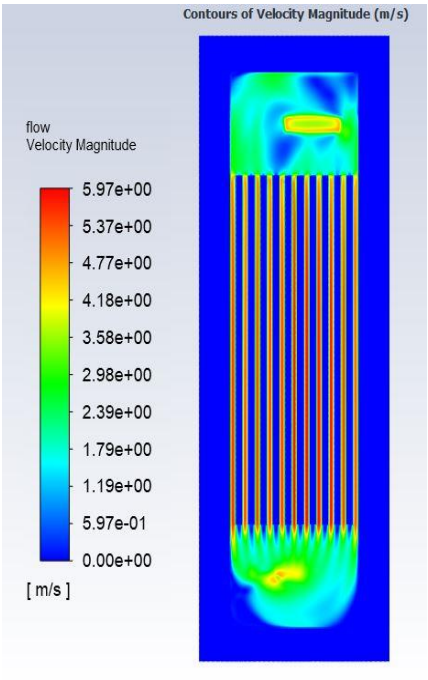

Figure 5: Turbulent intensity

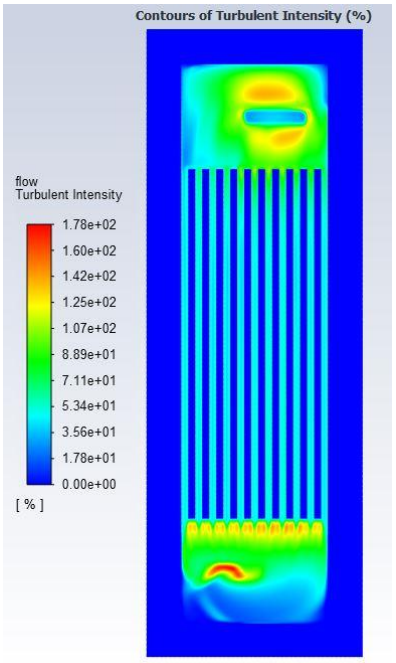

Figure 6: Velocity inside the microchannel

To demonstrate the effect the geometry has on the flow field and flow state, the laminar and turbulent temperature graphs of the fluid are shown in Figure 5 and Figure 6, respectively. It can be seen that the laminar temperature never converges as the temperature never reaches a steady state, while in the turbulent model, temperature does settle.

The turbulent Intensity factor plotted in Figure 5 is a clear indication that turbulence is present in the flow. If the inlet and outlet are ignored, however, the flow inside the channels remains laminar. This is a gratifying result, as all validation graphs and values are modelled in the channels. As the results of Abdollahi et al. (2017) are achieved with laminar settings and the Nusselt and pressure drop is calculated inside the channels, the research data in this study will still be valid and verifiable against their data.

3.3 MESHING

3.3.1 Introduction

The mesh required in flow analysis using Ansys Fluent is an imaginary, superimposed pattern used to fix data points for computation relative to the physical geometry

Structuring the mesh to ensure the independence of the solution is critical. Mesh independence is a term used to indicate that the mesh has no influence on the solution. The number of cells is calculated to ensure that the solution does not change if more cells are added. The basis of the mesh has to be structured with minimal orthogonality issues. Orthogonality is a quality measure of the mesh structure. Mesh quality shows how structured or unstructured a mesh is. A well-structured mesh with perfectly squared corners and no complex structures was used.

3.3.2 Meshing criteria

In selecting which mesh to use for the simulation, it is useful to consider the meshing criteria:

- The mesh must be structured.
- The overall quality of the mesh must be sufficient (good quality yields consistent results).
- The mesh geometry must not slow simulation (mesh type influences the solving time of the solution).
- The mess geometry must be simple (meshing can take up a lot of time; a less complex mesh will be generated faster).

Meeting the abovementioned criteria ensures that the experiment can be repeated with the same results and that the best possible solutions are reached with minimal errors between cells.

There are three mesh types to choose from in Ansys Fluent: tetrahedrons, hexagonal mesh and Cartesian mesh. Some of the tests and metrics performed on the different mesh types to determine the best mesh to use are given below.

3.3.3 Mesh types

Tetrahedron meshing

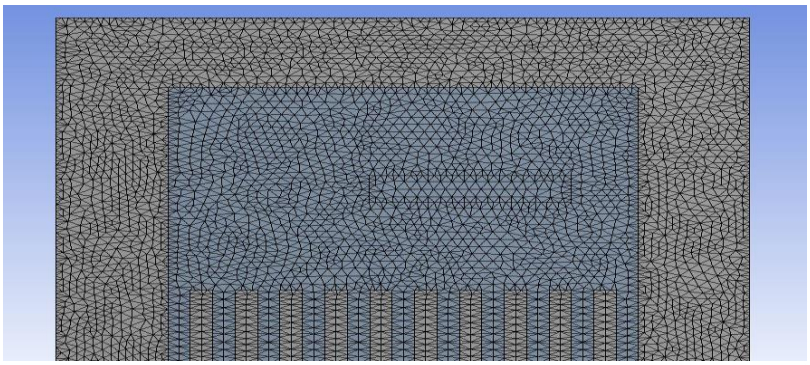

Figure 7: Tetrahedron meshing

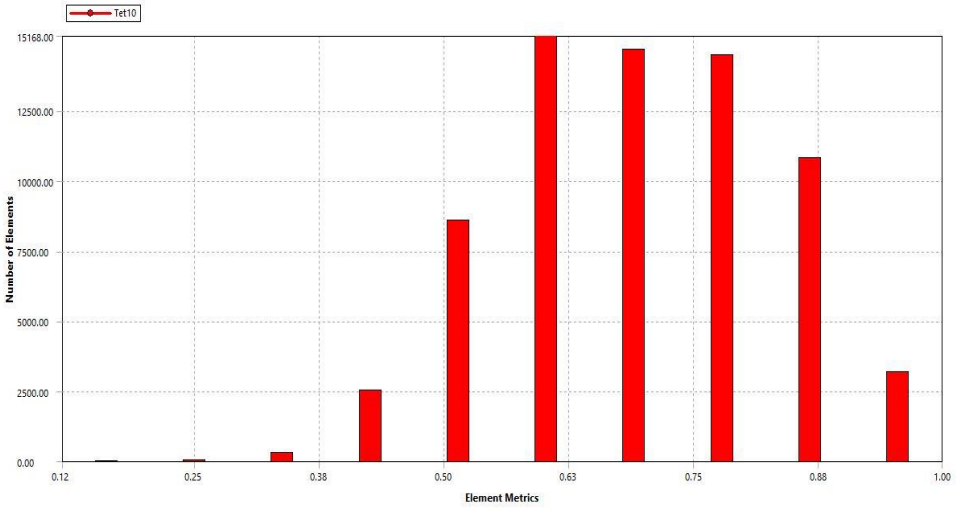

Figure 8: Number of cells vs mesh quality for tetrahedral mesh

Tetrahedrons**Error! Reference source not found.** are some of the more complex meshes to simulate. The mesh needs a lot of user input to define boundary layers and to ensure the proper quality is reached in all sections, as the Ansys Fluent default mesh options do a very poor job of refining the mesh. The mesh quality is poor, having a median quality of around 63%, as seen in Figure 8. This figure gives a distribution of the number of cells and the quality of the cells. The quality of a tetrahedron mesh is often not satisfactory without a lot of user input and refining.

Hexagonal meshing

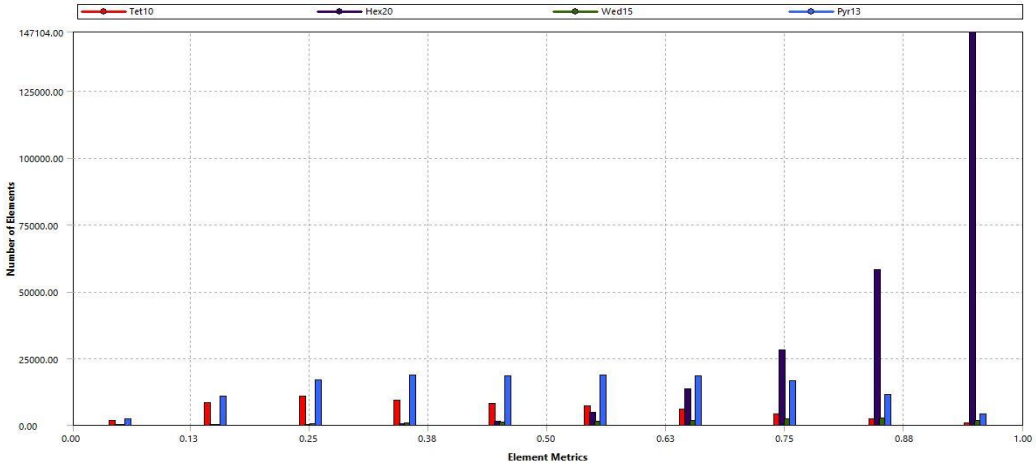

Figure 9: Number of cells vs mesh quality for hexagonal meshing

The hexagonal mesh simulated in Figure 9 is of a very bad quality. A hexagonal mesh is created by adding hexagons where possible. This means that four different cell groups are created: tetrahedrons, hexagons, wedges and prisms. This adds to the complexity of the mesh and removes a lot of the quality. All the hexagon cells have a great quality. However, the addition of prisms and wedges is detrimental to the overall quality of the mesh. This mesh requires a lot of creation time. The mesher has to iterate over the mesh a few times to ensure that hexagons are added wherever possible. The transition between different cell types makes for cells with a very poor overall quality, having skewness and shape distortion.

Cartesian meshing

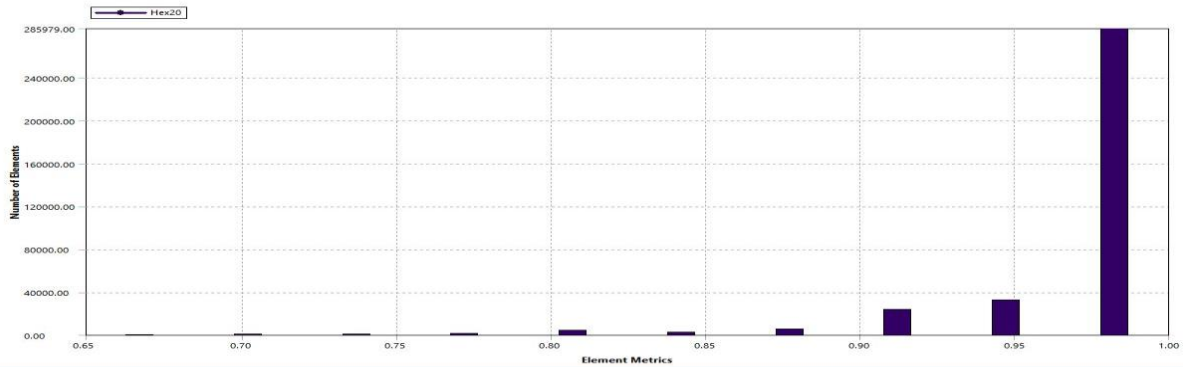

Figure 10: Number of cells vs mesh quality for Cartesian mesh

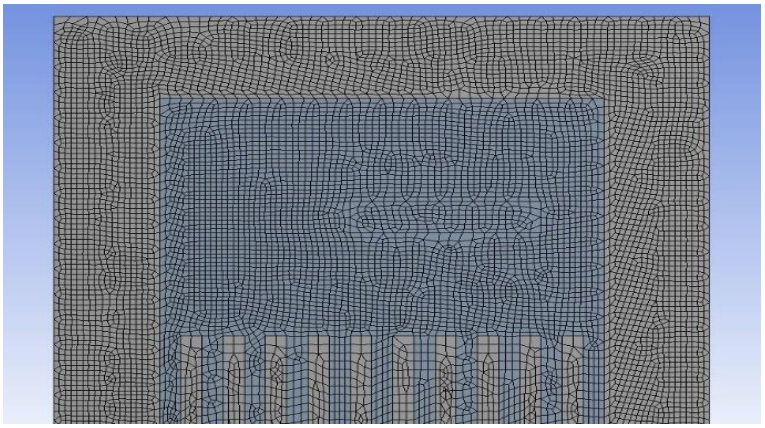

Figure 2: Cartesian meshing

The Cartesian mesh type is a very clean mesh setting. Figure 11 shows the mesh to be very consistent. The mesh quality is far better than the hexagonal and tetrahedron meshes and it consequently requires much less simulation time. This is the fastest mesh type as the mesh operations take place in record time compared to the other mesh types. A mesh with better quality overall means more consistency between cells and a more accurate transfer of the calculated data through cells.

3.3.4 Chosen mesh type

It is evident that cartesian meshing is the preferred mesh type.

Table 1: Mesh metric comparison

Mesh Type	Structured	Quality Median	Solve Time	Complexity
Tetrahedrons	No	0.63	Medium	Medium
Heagons	No	0.95	Slow	Extreme
Cartesian	Yes	0.977	Fast	None

Table 1 shows that the structured Cartesian mesh is the superior mesh in terms of having the best overall quality and very fast solving time. The Cartesian mesh is the best in each category.

3.3.5 Wall functions

Introduction

The setup of the geometry and the models used to quantify the material properties of nanofluids have to be solvable in single-phase laminar flow This is done to expedite the solution time, as running many different design points can become unfeasible as it is not possible to solve them in a reasonable amount of time on a standard university computer. With the realisation that the simulation still had some turbulent flow around the inlet and outlet, the simulation was changed to turbulent flow.

Turbulent flow is increasingly affected by walls and channels. The no-slip condition set on the walls influences the mean velocity field in the channels. The turbulence is influenced by wall presence in non-trivial ways as well. Extremely close to the wall, viscous damping reduces tangential velocity fluctuations, while kinematic blocking reduces the normal fluctuations. Near the very outer part of the turbulent wall zone, the turbulent kinetic energy -is increased by large gradients in the mean velocity.

Near wall modelling impact on the accuracy of any numerical simulation. As walls are the main source of turbulence and subsequent vorticity, Thus, accurate representations have to be added in any near-wall situation. The literature defines wall functions and near-wall functions (Park and Lee, 2018). Fortunately, wall functions and near-wall models are both supported by Ansys Fluent Each type works best with certain turbulence models. The Ansys Theory guide was thus consulted for accurate information (Ansys, 2013).

Wall functions vs near wall model

Wall functions

When wall functions are used, the viscosity affecting the inner subregions is not simulated in detail, but is bridged by semi-empirical formulas. In turbulent flow regimes, wall functions can be utilised to account for channels and walls.

Near-wall model

When using a near-wall model, the model is resolved with a fine enough mesh to track the turbulent regions accurately. Considering the viscous sublayer, an extremely fine mesh has to be used.

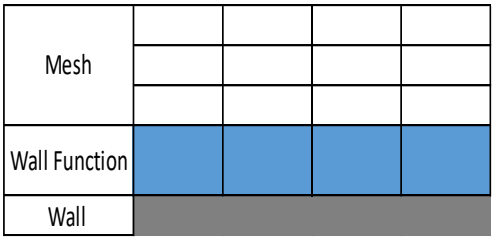

Figure 3: Wall function depiction

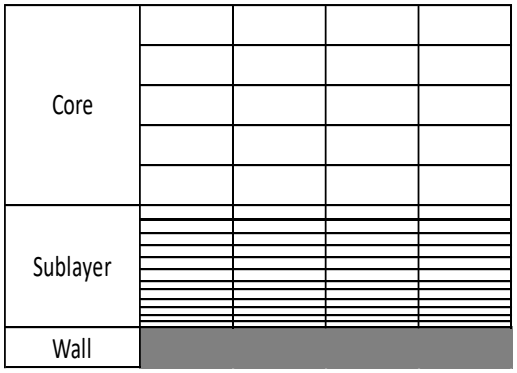

Figure 4: Near-wall model depiction

As indicated in figures 12 and 13, the near-wall model can be seen as a refined mesh. The wall functions bridge this sublayer with semi-empirical formulas. If a near-wall model is chosen, the cell count will more than double as this mesh refinement occurs in channels against all walls. As increasing the number of calculation cells will dramatically increase the simulation time, it was elected to use

wall functions instead. The following section will show the wall function method chosen and some restrictions and wall function suggestions for use.

Wall function use and restrictions

Wall functions seem like the optimal method of calculating near-wall situations as the mesh does not have to be as refined to have the same output accuracy. A drawback of wall function is that results deteriorate with refinement of the mesh. A coarse mesh is needed next to the wall, with complications if the coarse mesh influences another region that needs fine mesh.

Y-plus (y^+) is a quantification of cell size and mesh refinement statistics, calculated as shown in Equation 21. Y-plus values of less than 15 will influence the results negatively.

$$y^+ = \frac{\rho u_t y}{\mu} \tag{21}$$

where ρ is the density of the fluid, μ is the viscosity, y is the absolute distance from the wall and u_t is the friction velocity.

Figure 14 depicts the y-plus value in the mesh used in this project for the actual simulation, showing that the average near-wall y-plus value of the mesh is 14.8 (<15). That is close enough to 15 to ensure accuracy of the wall function. It can also be seen that the y-plus values inside the channels where the wall functions are applied are also large enough.

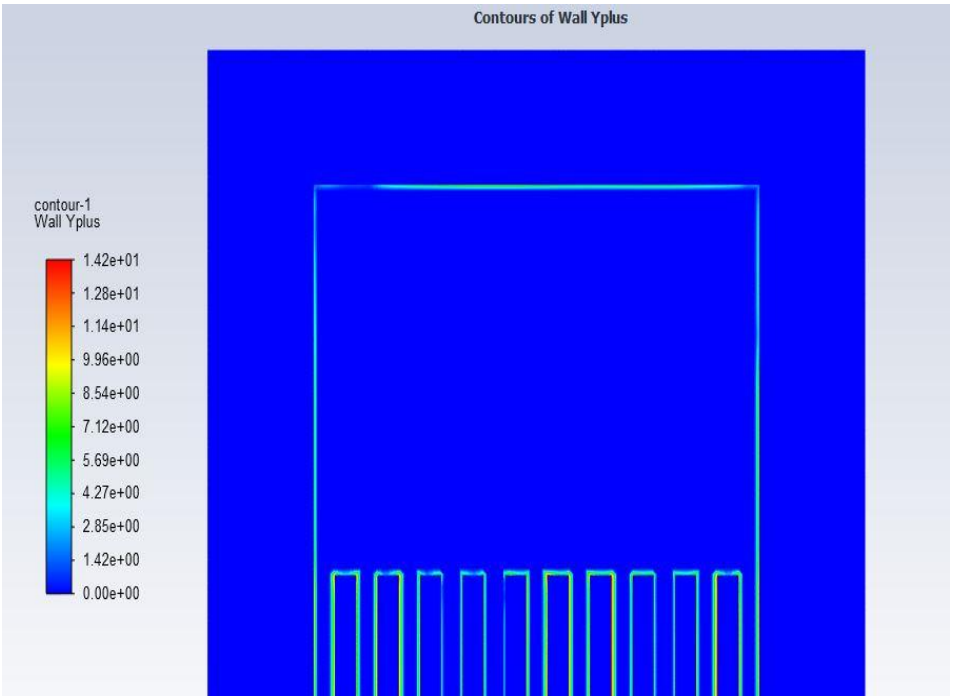

Figure 5: Y-plus values for the mesh

Ansys's theory guide recommends some wall functions for certain turbulent models. For the required k-e turbulence model, either Menter-Lechner or enhanced wall functions are recommended. It was decided to do a small study to determine which of the two recommended function gives the best results, preferably in the shortest time. This was done as accuracy and simulation time are based on the geometry and the mesh, and are case specific.

Table 2 shows the number of iterations required to reach a fluid temperature accuracy of 10^{-8} C for the Menter-Lechner and enhanced wall functions respectively. This was done to ensure that a comparison can be made between design points, as the accuracy of each simulation is exactly the same. This meant that accuracy would influence the results, taking another variable out of the system, as a comparison between the design points will determine the optimal point in the system.

Fifteen design points were taken and each was simulated, first with the Menter-Lechner wall function and then with the enhanced wall function. If less iterations are used to reach the convergence point, that method is considered better as it lowers simulation time, while the accuracy is exactly the same with the new convergence criteria added.

The results of the comparison indicated that the enhanced wall function delivers better results than the Menter-Lechner function.

Table 1: Wall function time comparison

Type	Menter Lechner	Enhanced Wall Functions
Design Point	Iterations	Iterations
1	350	275
2	348	292
3	363	296
4	385	263
5	374	298
6	378	287
7	360	269
8	347	284
9	327	270
10	375	261
11	330	251
12	359	286
13	347	272
14	367	275
15	338	298

3.4 ANSYS FLUENT

3.4.1 Introduction

The following section details the settings and configurations that had to be done in Ansys Fluent to ensure that the design point system would work. The aim is to use a single Ansys Fluent setup and duplicate it throughout the Workbench design point workspace. This lets one simulate the different material and fluid combinations of nanofluids in one simulation and Workbench setup, which condenses the post-processing stage in a single file. The setup will be shown below, as well as the problems encountered and the fixes applied, as Ansys Fluent is inclined to generate bugs when more than 10 design points are used.

3.4.2 General setup

Type of solver: pressure based

Pressure-based solvers are chosen for low Mach number simulations or incompressible flow simulations. As the instance that has been created conforms to these criteria, the pressure-based solver was chosen. Pressure-based solvers work by acquiring a Poisson equation using the continuity and momentum equations. This is then implicitly resolved, neglecting acoustic time scales because of the Mach = 0 assumption.

Velocity formulation: absolute

Absolute velocity is chosen when the fluid in a geometry is not rotating., as the relative velocity formulation would add two additional acceleration components to the momentum equations to ensure that vorticity can be resolved. (Ansys, 2013)

Time setup: steady state

A steady state time setup is chosen as no mass transfer is present in the system. The system will eventually reach a state where the heat transfer will stop heating the fluid and the channels will only cool the solid to a certain temperature.

3.4.3 Solver setup

Energy: on

The energy setting needs to be on for any heat transfer to be simulated in the system. If this setting is off, the only resolvable equations would be based on fluid flow. Although the velocity and pressure can be seen, temperature would not be indicated.

Viscous settings: standard k-e model with enhanced wall functions

Enhanced wall functions were described in depth in Section 3.3.5. The standard k-e model is used as it is the most experimentally validated model. This function adds two transport equations: calculating the turbulent kinetic energy and the kinetic turbulence rate of dissipation. As only the initial conditions and boundary conditions are needed for this model, it is one of the simplest models.

3.4.4. Materials

Solids

The only solid in the geometry is the silicone base of the microchannel. This was set up by entering the respective material properties into Ansys Fluent as everything stays constant.

Fluids

The optimisation challenge that was set for this project was that the inputs and outputs of the system should be clearly visible and comparable with other data points. This would then be used in an optimisation algorithm that would find the optimal point in the system respective to the Nusselt number and pressure drop. This meant that the inputs (nanoparticle, base fluid, diameter of particle and concentration of particle) that represent the material properties of the system had to be shown with the respective Nusselt number and pressure drop for that simulation. Ansys Workbench offers a parameter system where inputs and outputs can be seen in a tabular format. The advantage of this is that the setup can be easily tested. Inputs can be checked and verified by the code written for the calculation of the material constants. The output of the Nusselt number and pressure drop can then be verified by comparing and validating the data of Abdollahi et al. (2017).

The setup works as follows and in the sequence shown:

Python script

Constants for the material property models described in Section 2.4 were calculated and converted to a text file. The script was designed to compute each of the 256 possible combinations of selected

inputs to generate density, viscosity and specific heat. The script was set up so that the different inputs could loop through all the iterations in sequence, substituting them in the material properties models Other constants were also defined in the user defined function (UDF) to calculate thermal conductivity. This was done so that all the calculations could be presented in one script without having to combine answers from a possible C++ script (the language used by the UDF). This meant that the UDF only needed to manipulate constants and then add the changing temperature and output to Ansys Fluent to calculate the heat transfer as the system converged. A sample of the code will be shown below to demonstrate how it works. The inputs are the material properties and the optimisable variables, concentration, base fluid, nanoparticle and diameter. The calculations are substituted into the material properties models and the output is the text file. Constants are converted to Ansys Workbench parameters.

Problems encountered

The biggest problems encountered with this method of coding and the method used to get all the different iterations was the fact that material properties ended up being the output. This meant that one material property might have three different main inputs inserted into the equations. This made it very difficult to check if the code actually worked. It could not be observed whether the output had any direct comparison, which made it difficult to determine which particle concentration, nanoparticle or base fluid to use in the calculation. As coding works with only numbers and iterations, it is extremely important to check and validate the output to ensure a trustworthy code. A lot of time would be wasted if the researcher was thus to think that the design points are correct and was to spend a few days simulating them, only to discover in post-processing that the inputs were incorrectly matched.

Solution

The easiest way to solve the problem was to do some hand calculations to validate the code. This was done for the first ten design points. The order was saved by adding an extra output to the system. Each time an input was used in an equation, that input was added to a list. This meant that the perfect order was saved for each design point, giving assurance regarding which input was connected to a certain output in the simulations. This extra list was not added to the Workbench environment, as it had no influence on the system. It was later captured in Excel and filtered to check that each element had 64 iterations of the specific input being used. Each category had four inputs and there were 256 design points in total if every combination was calculated. This then meant that each input would have 64 design points. Every iteration was done correctly in the intended order.

Workbench Journal File

Certain problems were encountered and solutions generated, including the option to record a Workbench journal file. These are discussed in the section below.

Problems encountered

Creating design points in Ansys Workbench is a functionality that was added to easily compare results when inputs needed to be changed. This parameter set contained the solution for multiple simulations at a time, making comparison easy. Creating these design points can be a very labour-intensive exercise. One has to right-click on the original and select "duplicate". All the inputs would then be exactly the same as the original design point and would have to be changed manually to the new input values. Right-clicking and changing the values to a new set manually would take ages and make the project redundant. It was thus decided that an automatic method would need to be used to insert all the constants calculated in the above Python script into the different design points.

This would enrich the methodology considerably, as it meant that any inputs could be added to the code and simulated. This would be especially relevant when adding new materials or fluid surfaces in the field to the system to compare them with previous data. This meant that any base fluid, nanoparticle, concentration and diameter could be added to the system for comparative purposes.

Solution

In Ansys, the option to record a journal file was added. A journal file records all user inputs. In Ansys, such a file can be run again and the same actions will be performed automatically for the user. This method has some limitations as the interface in which the journal was recorded has to be open, otherwise it will not find the buttons.

After converting the material constants into parameters, they are simply exported to Ansys Fluent with the respective properties. The journal file also creates all the design points from the constants, which creates the design study of all the parameters and different combination of inputs needed for the optimisation phase.

A journal was thus recorded where the design point was duplicated and each input changed manually. The journal was stopped there, and this code copied into Python. The idea was that the researcher could use the calculations of all the design point inputs and copy them into the new journal entry. This entry could then be used and copied into a text file 256 times using a loop in Python, essentially, making a journal file that contained 256 duplicate commands. This worked extremely well, as when the journal file was run in Workbench, all the desired design points were created in seconds.

This meant that the system was automated and any input could be inserted into the code. Creating a journal file that could be run in Workbench made it possible to create as many design points with the desired inputs as needed.

Ansys Fluent UDF

A UDF was used to create the temperature-dependant variable of the thermal conductivity, as this is the only method that Ansys Fluent has for adding specialised variable functions.

Workbench parameter set

When activated, Workbench will solves the design study by solving all the design point and then moving on to the next after updating and saving each design point's converged data. The design study can then be completed with all the answers in one space where comparison can easily be done. This helps with the initial state of data interpretation as it will already show trends in the data and ensure that the simulations were done correctly. The parameters in Workbench were set up so that the inputs could be changed, and the outputs seen immediately. This meant that the four inputs that needed to be changed for optimisation purposes had to be input into the system. All the data for the inputs therefore had to be calculated before the parameter set was even created. e In section 2.4, the reasons for using the models of Koo and Kleintrauer to create the parameters in Python were given. The inputs into the parameter set will be shown below. The configuration to connect some of the input parameters to a UDF file used for thermal conductivity needed to be temperature dependant. As a parameter set cannot just be created, all the parameters must be linked to the correct parameters in Ansys Fluent to ensure that, if a density is added, Fluent understands that the density has been changed, and thus applies the change and ensures that the units are correct.

3.5 CONCLUSION

This chapter presented the methodology used in this study, and explained how Ansys Fluent works. An explanation was also given regarding what needed to be done to ensure that the data was created in a usable way, which could be easily extracted, after the simulations had been done. The Workbench parameter set method was chosen as the implementation method, as it allows the user to duplicate the flow field and mesh by only changing the inputs to the material properties of the fluid. This ensures faster simulation times and efficiency as a great number of simulations are run to create enough data points in the design study to have good enough optimisation results. The next chapter will detail all the simulations that were done and their results, starting with the simple simulations and proceeding to the full design study.

This shows that the design study was not just created. Steps were followed to ensure that each section of the simulation could be verified. This meant first checking how to ensure an optimal mesh that captured all the heat transfer data, and then solving the flow field correctly with the correct inputs to Ansys Fluent, like wall functions and turbulence models. The researcher could then progress to implementing a nanofluid, as the previous simulations were done with water as fluid. The simulation was then duplicated to see how this works and what Ansys Fluent can handle in terms of automatisation. The design study was finally created and tested again for accuracy.

CHAPTER 4: RESULTS AND DISCUSSION

The necessary theoretical knowledge was gained through the literature study as well as the practical implementation of the simulations has been done. The following section will detail the results obtained from f the simulations and optimisation. The theme of optimisation was kept through the entire project as everything had to be chosen in order to ensure that the optimization section of the report flowed well and was not complicated unnecessarily as optimization as a topic is already complex enough. The models chosen to characterize the material properties where chosen to ensure enough parameters could be changed. This led to more possibilities and thus more iterations of different combinations of inputs. This allows a bigger design study. A bigger design study is very important for optimization, if not enough data points are available optimization cannot be done.

The chronological steps in the implementation of the study were as follows:

1. Validate a nanofluid simulation with numerical and experimental results
    a. Show the timeline of simulations from 2D to 3D, from only water to the implementation of the nanofluids
2. Design study
    a. The design study includes what nanofluids were added and the contribution of this paper to the field, i.e. the setup of the full design study for optimisation to be viable.
3. Optimisation
    a. Detailing what methods were used and what was done to characterise the design study in order to ensure that the design point's simulations only had to be done once, as a regression algorithm could then predict the same outcome from the inputs as the actual Ansys Fluent simulation. The optimisation is then done on this function and not in Ansys Fluent, as this would require having to wait for a simulation again. This reduces time and improves the efficiency of the model.

The objective with this section is to detail what simulations and optimisations were done, and to present the results in a clear, concise way.

4.1 VALIDATION OF THE NUMERICAL RESULTS

4.1.1 Introduction

Validation of results is extremely important for this thesis, as all results shown are purely numerical. This entails that a reference point had to be made that has been shown as correct with experimental data. If new simulation configurations then match this point and completely describe the flow field at this point, all data is seen as valid. This reference point can then be built upon in new studies.

The order of validation starts at a simple level and then proceeds to become more complex, as 256 different combinations of nanoparticle, diameter, concentration and base fluid was simulated for the design study. This was then characterised with a Radial Basis function (RBF) and optimised using a neural network and General algorithm.

In order to get to the complex simulations, the following structuring was used in order to understand and validate each individual section of the simulations.

1. 2D case
    a. Using water:
        i. to determine the mesh density needed for each channel in the microchannel system.
2. 3D case
    a. Using water:
        i to determine if the flow regime and boundary conditions are set up correctly.
3. Nanofluid case
    a. Using a nanoparticle and water as base fluid
        i to determine if the material properties were solved correctly as this was done with non-constant parameters; for instance, the thermal conductivity was temperature dependent.
4. Design study
    a. Multiple simulations
        i changing the material properties of each design point while keeping the flow regime, boundary conditions and mesh constant; only the inputs (base fluid, nanoparticle, diameter of particle and particle concentration) were varied.
5. Optimisation
    a. Optimise the design study
        i Some 256 different points were created using different inputs, all with different outcomes; optimisation was performed to determine the highest Nusselt number and lowest pressure drop to allow the best heat transfer, while also ensuring that the pump uses as little energy as possible.

4.1.2 Validation results

Conservation equations

All the simulations kept the same boundary conditions and flow regime. This is explained with the governing equations below, as well as how some of the performance-identifying parameters were calculated (pressure drop and Nusselt number). The following assumptions governed the model and simulations:

1) The channel reaches a steady state.
2) The turbulent k-e model with enhanced wall functions is applicable
3) A Newtonian fluid is used.

4) Nanoparticles and base fluid are in thermal equilibrium.
5) The fluid is in a single phase
6) The properties of fluid flow in the microchannel are constant and temperature-independent

(Azimi and Kalbasi, 2014; Abdollahi et al., 2017)

Following the assumptions made, the following equations can be set out and used in Ansys Fluent.

Continuity:

$$\nabla \cdot \vec{V} = 0 \tag{22}$$

Momentum equation

$$\rho\left(\vec{V} \cdot \nabla \cdot \vec{V}\right) = -\nabla p + \mu \nabla^2 \vec{V} \tag{23}$$

Energy equation for fluid flow

$$\rho C_p\left(\vec{V} \cdot \nabla T\right) = k \nabla^2 \vec{V} \tag{24}$$

Energy equation for solid section

$$k_s \nabla^2 T_s = 0 \tag{25}$$

The following equations will be calculated in Ansys Fluid to keep track of the equations for Nusselt number and pressure drop:

From the turbulence model, two extra equations are added to calculate the turbulence.

Turbulent kinetic energy: k

$$\frac{\partial(\rho k)}{\partial t} + \frac{\partial(\rho k u_i)}{\partial x} = \frac{\partial}{\partial x_j}\left[\frac{\mu_t}{\sigma_k}\frac{\partial k}{\partial x_j}\right] + 2\mu_t E_{ij} E_{ij} - p\varepsilon \tag{26}$$

Dissipation rate: ε

$$\frac{\partial(\rho \varepsilon)}{\partial t} + \frac{\partial(\rho \varepsilon u_i)}{\partial x_i} = \frac{\partial}{\partial x_j}\left[\frac{\mu_t}{\sigma_\varepsilon}\frac{\partial \varepsilon}{\partial x_j}\right] + \frac{C_{1\varepsilon}\varepsilon}{k} 2\mu_t E_{ij} E_{ij} - c_{2\varepsilon}\rho\frac{\varepsilon^2}{k} \tag{27}$$

with

u_i = the velocity component in the corresponding direction

E_{ij} = the component of rate of deformation

μ_t = the eddy viscosity

$$\mu_t = \rho C_\mu \frac{k^2}{\varepsilon} \tag{28}$$

Reynolds number:

$$Re = \frac{\rho u_{av} D_h}{\mu} \tag{29}$$

Nusselt number:

$$Nu = \frac{h(x) D_h}{k} = \frac{q_w D_h}{k(T_w - T_b)} \tag{30}$$

$$Nu = \frac{h D_h}{k} = \frac{q_w D_h}{k(T_{hs} - T_{ave})} \tag{31}$$

Pressure drop:

$$\Delta P = \frac{1}{2} \rho F Q^2 \tag{32}$$

(Abdollahi et al., 2017)

Equations 28 to 32 will be validated with previous literature results in order to accurately track the performance of the model being set up. Ansys CFD is a very detailed simulation program that can resolve very complex flow. This adds to the complexity of validating the research findings with previous work as some of the specifics are not always mentioned. The above equations will help to identify where a faulty method is being used. As a result of the multitude of parameters, the configuration of the ANSYS simulation had to be iterated to ensure that the validation could be done.

Case 1: 2D water

Model

Firstly, a 2D case was developed to ensure that the correct flow is resolved inside the microchannels, emphasising the flow inside the channels as this is where the Nusselt number and pressure drop will be primarily calculated for validation. Mesh pattern selection is important in ensuring accuracy.

The model was built in SolidWorks as a CAD to ensure that the dimensions were as close to perfect as possible. The model was then imported into Ansys. A Cartesian mesh was implemented as it provides the best cell quality. The geometry is perfectly square with no rounded or abstract edges, which means that the mesh can perfectly define the entire geometry. An in-depth discussion on mesh implementation was provided in Section 3.3. The first case has a geometry of one of the microchannels, with L = 10 mm, H = $400\ \mu m$ and B = $200\ \mu m$.

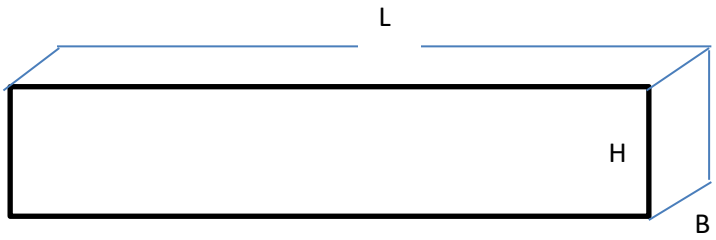

Figure 15: One microchannel base case

The initial simulation of only one channel is done to ensure that mesh independence is achieved inside the channels. This way some mesh refinement can be done inside the channels to lower the cell count. The cells being saved inside the channel where laminar flow is present can be used at the outlet and inlet where more complex flow is present. It was seen that the V-type inlet required more cells to solve the equation at the inlet and outlet as turbulent flow is present, where, as predicted, the channels had laminar flow.

Setup

- 2D base case
- Laminar flow
- Heat transfer added to the bottom boundary 100 W/cm^2
- Velocity of 5 m/s (Reynolds number of 1 333)

Grid independence testing

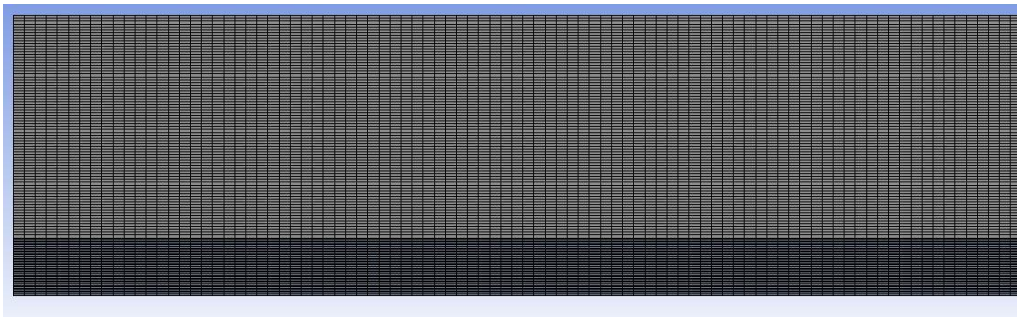

Figure 16: 60 000 cell mesh in 2D case

This first base model will be used to ensure that mesh independence is reached. This will help with the quantification of the 3D model. A simple geometry was built as described above. In the simulation, three different meshes were tested and the temperature of the channel of each mesh was recorded to see if independence had been reached inside the channel. The following cases were analysed and reported. Parameterisation was done in Ansys Workbench to ensure that the reports and graphs can be generated automatically.

The parameters were divided into three sections: the vertical number of divisions, the horizontal number of divisions for the solid and the horizontal number of divisions for the fluid.

Table 3: Design points

Name	P2 - Vertical Number of Divisions	P3 - Solid_Horizontal Number of Divisions	P5 - Fluid_Horizontal Number of Divisions	P4 - Mesh Elements
DP 0	100	4	12	1600
DP 1	150	10	20	4500
DP 2	200	20	40	12000
DP 3	500	40	80	60000

For the following design points, the case was resolved and the temperature graph plotted. The average temperature is listed in Table 4. It was seen that mesh independence from the different cell counts was already reached at the 12 000 cell mark. This implies that to correctly model one channel, 12 000 cells are needed. This was later incorporated into the 3D model to ensure optimal computational time for the simulation.

Table 2: Mesh elements vs temperature

Design point	Mesh elements	Average temperature (K)
1	1 600	303
2	4 500	304
3	12 000	306.15
4	60 000	306.21

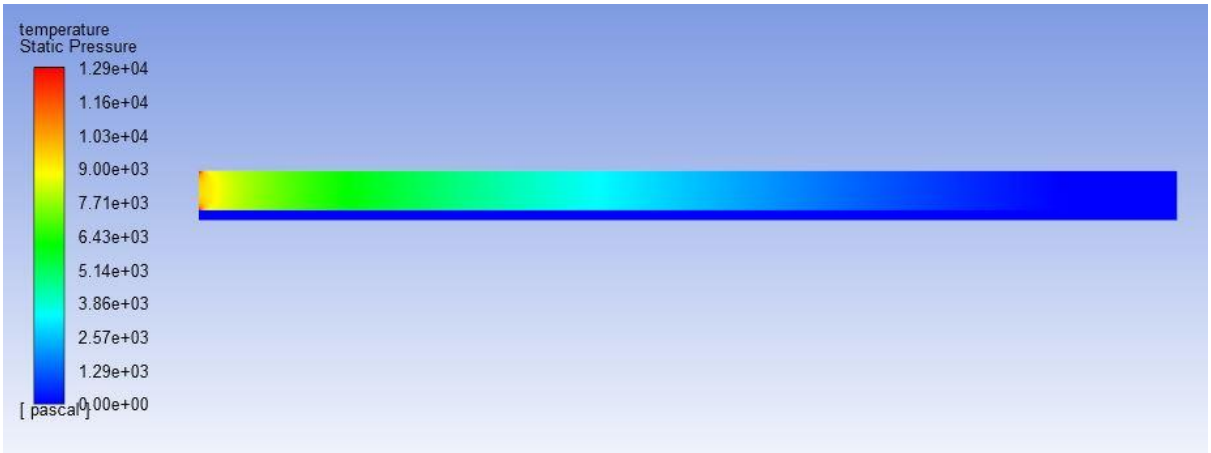

Figure 7: Pressure distribution in the 2D case

One of the solutions is depicted in figures 17 and 18 to show the simulation.

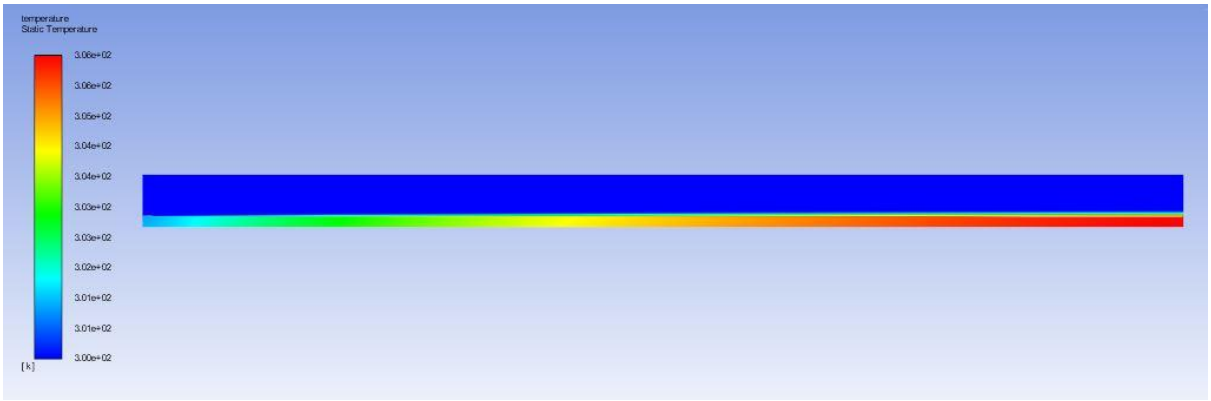

Figure 18: Temperature distribution in the 2D case

Conclusion

It was seen from the Grid Conversion Index (GCI) that using 12 000 cells per channel would not compromise the accuracy of the experiment. It is therefore not necessary to use 60 000 cells. This method ensures that the computational time is kept to a minimum for each stage of the simulation. As multiple simulations will be run later, this is of the utmost importance.

Case 2: 3D water

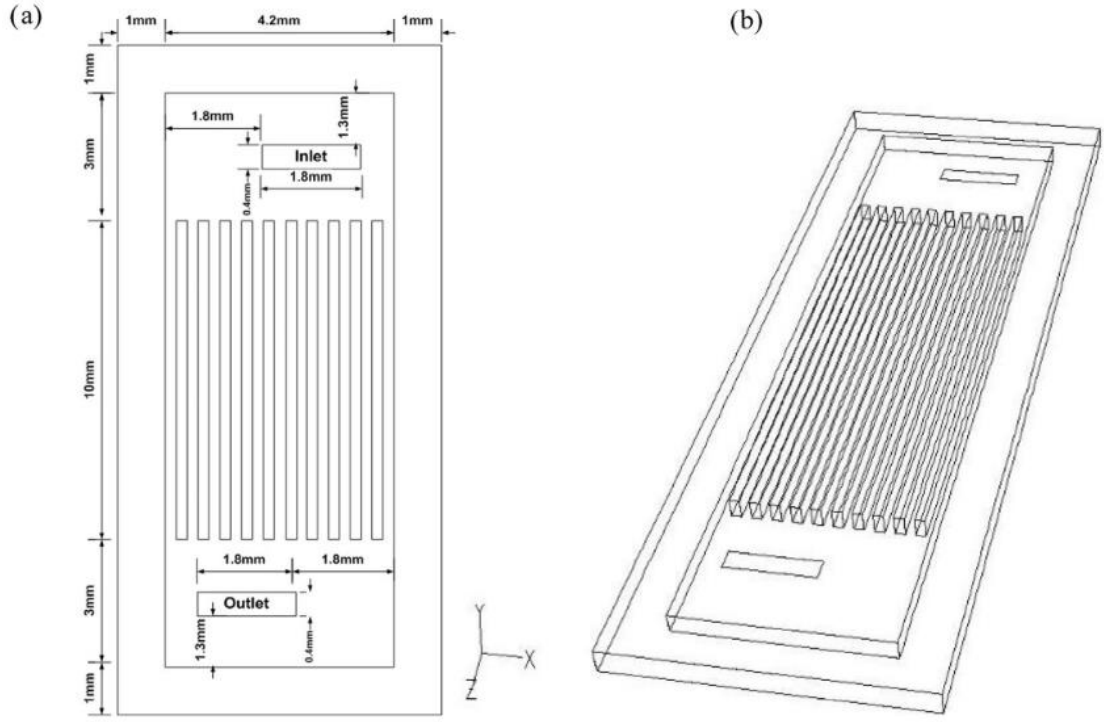

Figure 19: 3D model

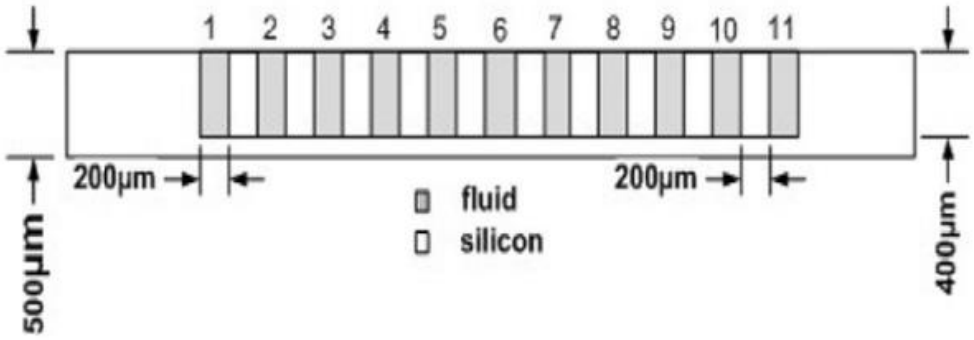

Figure 20: 3D model side view

Model

The full 3D model will be exactly the same as the model of Ayoub and Abdollahi (in Abdollahi et al., 2017), which followed the study of Chein and Chen (2009) on the inlet configuration of microchannels. As flow regimes are completely dependent on geometry, a standard geometry was chosen from the literature to validate the new model. This model is named a V-type inlet for the offset configuration of the inlet and the outlet of the channels. The channel is made from silicon.

The microchannel, as previously explained, will be used for the cooling of a CPU or computer component, therefore it is assumed that a constant heat flux will be applied to the bottom of the channel. The inlet and outlet are designed so that the flow will enter the system vertically. The flow will be completely laminar and fully developed inside the channels. However, turbulent flow exists at the inlet and outlet. The inlet condition of the flow speed is assumed to be relative to the fixed Reynolds number of 1 333 with an inlet temperature of 293 K. The outer walls of the microchannel are insulated, the base of the microchannel is being heated at a constant tempo of 100 W/cm^2.

Setup

- 3D case full geometry
- Turbulent flow using k-e model with wall functions
- Water as fluid
- Heat transfer added 100 W/cm^2
- Reynolds number at inlet of 1 333

Mesh independence analysis

Grid independence is measured with a GCI, as specified in Roach (1998), This method uses a performance parameter to determine if convergence has been achieved. For this partial model, the average temperature in each microchannel will be chosen as this can be compared to the results of Ayoub (in Abdollahi et al., 2017). Performance factors are calculated and used to ensure that the solution of the current mesh density is very close to or the same as the previous mesh density.

$$GCI = \frac{F_s \left| \frac{f_2 - f_1}{f_1} \right|}{r^p - 1} \tag{33}$$

If the GCI equals 1, grid convergence has been reached and the mesh refinement can terminate.

Table 3: GCI mesh independence

Design point	Mesh density	GCI
1	100 000	
2	150 000	0.767
3	250 000	0.864
4	350 000	0.923
5	500 000	0.976
6	1 000 000	0.9998

A total of 1 000 000 cells were used for this case as the amount of time that passed for the added accuracy was not that detrimental to the overall time. The 1 000 000 cell mesh was simulated in only 10 minutes due to the relatively simple flow field inside the microchannel.

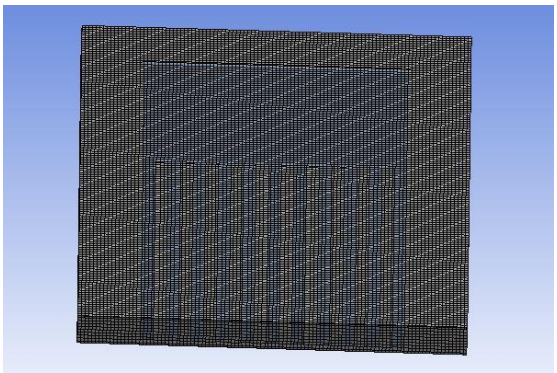

Figure 21: 3D mesh from the top

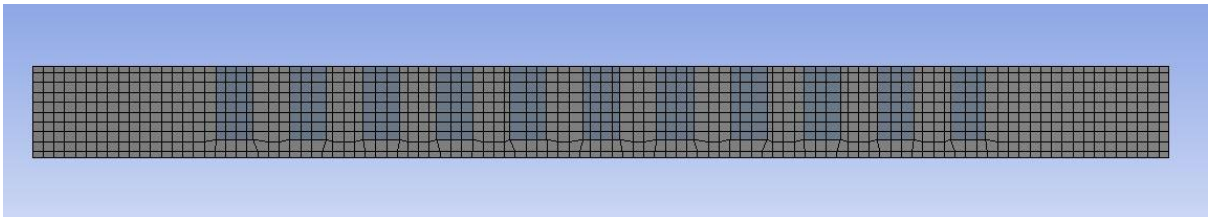

Figure 22: 3D mesh section plane

Results and validation

A comparison was made between the temperature contours of Chein and Chen (2009) and Ayoub (in Abdollahi et al., 2017), and the present work.

The result sets are compared in terms of average temperature in each channel to determine the measure or error between the different mesh qualities and simulations. This provides a good indication of the overall validity of the new model. The comparisons are presented in the graphs in Figure 25. The maximum deviation is one degree Celsius or 1.5% error This validation of the model is critical in ensuring that the foundation is modelled correctly. In the next section, a nanofluid will be simulated and the differences between the cases analysed. This base case will then form the foundation for the optimisation of nanofluids. Validation is done with water as fluid. Some difficulties were encountered, thus the validity of using only water was seen.

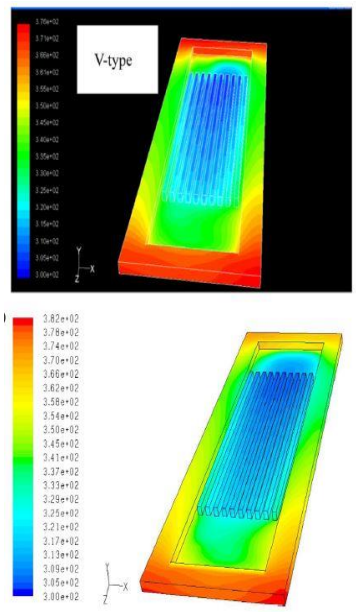

Figure 23: Top: Chein; bottom: Chen

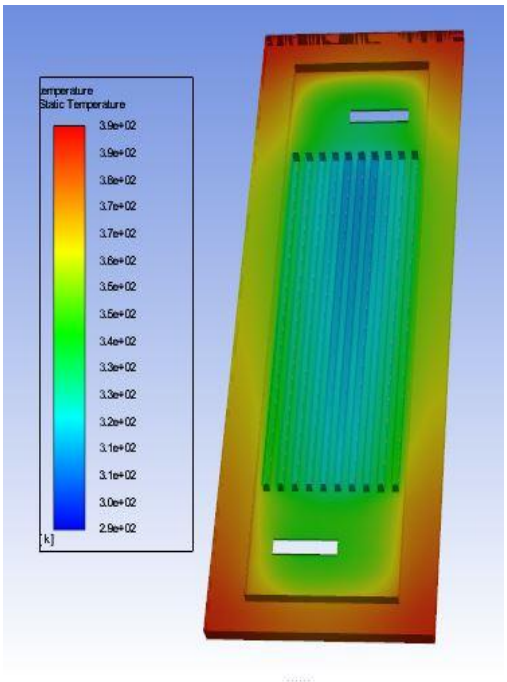

Figure 24: Present work

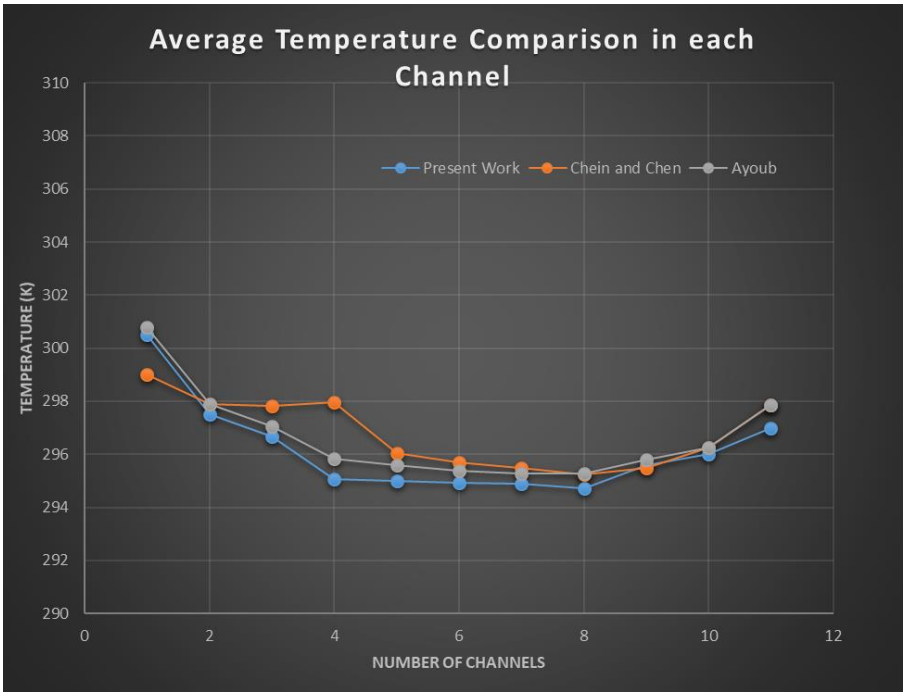

Figure 25: Water temperature comparison

From Figure 25, it can be seen that there was some very good correlation between the previous work and the present work. The validation that Chein and Chen (2009) had performed on experimental studies done by Phillips (1994) helped to confirm the validy of the geometry mesh and general model. This will allow further comparison with Ayoub (in Abdollahi et al., 2017), who also simulated nanofluids. Graphs and values are available for validation. The maximum error on the above graph will be shown in Table 6.

Table 6: Error comparison

Error %	1	2	3	4	5	6	7	8	9	10	11
Chein	0,693257242	1,328736442	0,561026	0,977711	0,672585	0,55732	0,499558	0,644881	0,672961	0,44929	1,537836
Ayoub	1,284058511	1,328736442	0,305557	0,264243	0,52225	0,451002	0,42862	0,66259	0,778995	0,44929	1,537836

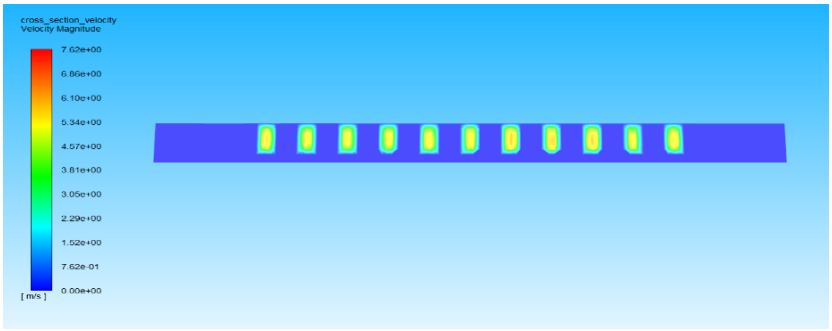

Figure 26: Velocity cross-section of vanes

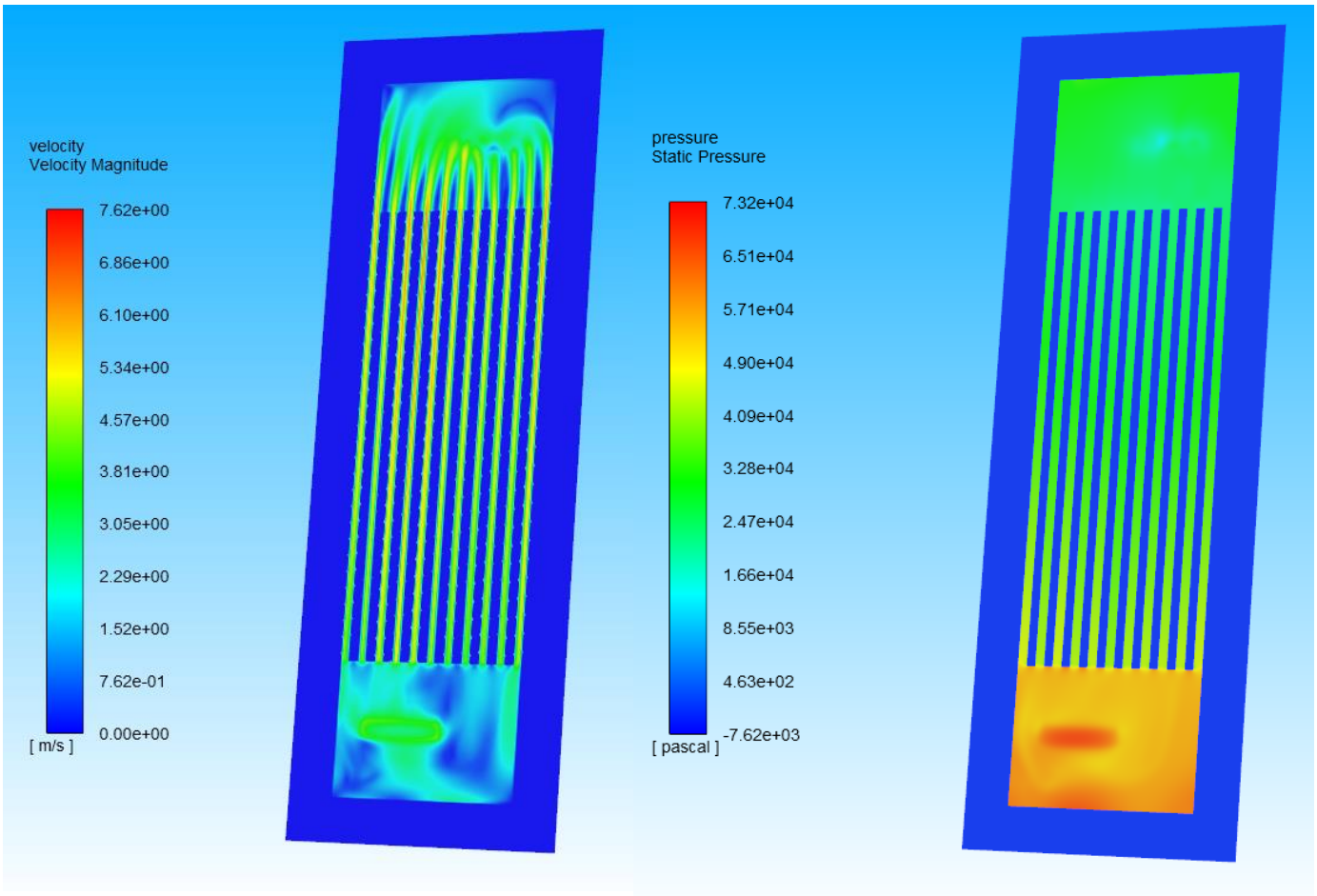

Figure 27: Velocity contour

Figure 28: Pressure contour

A complete overview is given of the simulation and the results that have been achieved. This is to show that the complete simulation has been run and data has been post-processed to compare it with previous literature. A mid-plane was created to show the best possible sections for creating contours.

In figures 27 and 28, it can be seen that the velocity and pressure contours conform to expectations, showing a high pressure at the inlet and a lower pressure at the outlet. The velocity contour has some exceptional quality and detail as the residuals for velocity in all three directions were down to 10^{-8}. The inlet is visible, as well as the velocity trails left by each channel at the outlet.

The following graphs show the velocity and temperature of each of the vanes. These were used in the comparison with the work of Ayoub (in Abdollahi et al., 2017) and Chein and Chen (2009).

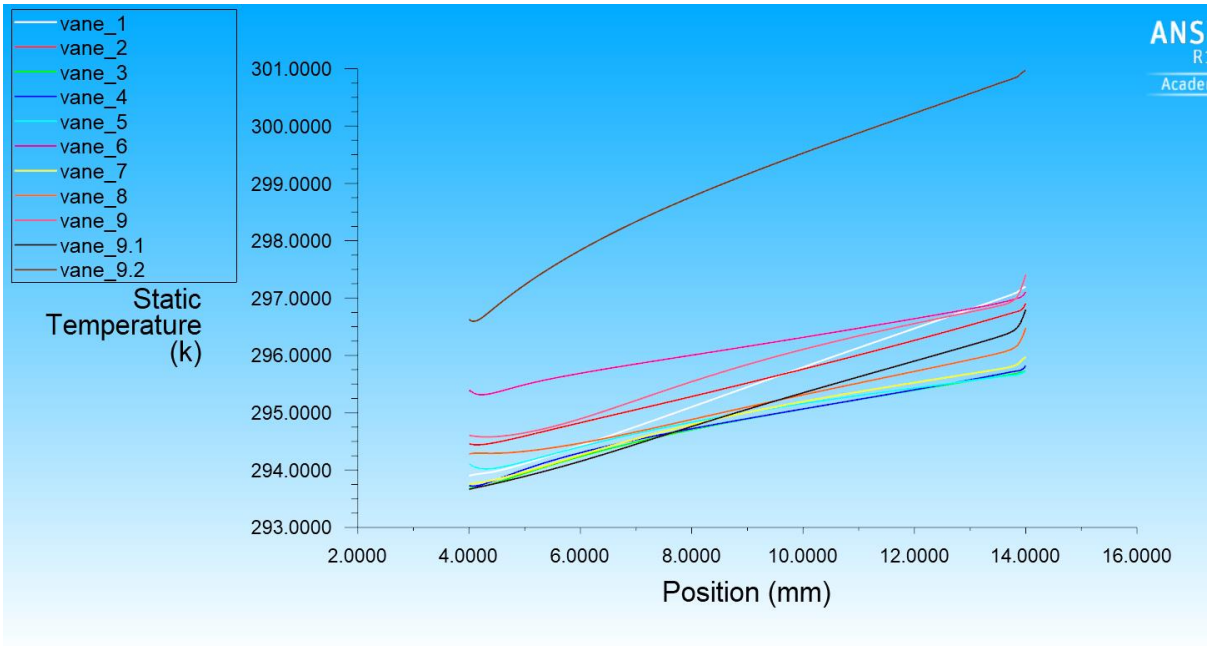

Figure 29: Temperature of each channel

The average of each channel's temperature was validated in Figure 29.

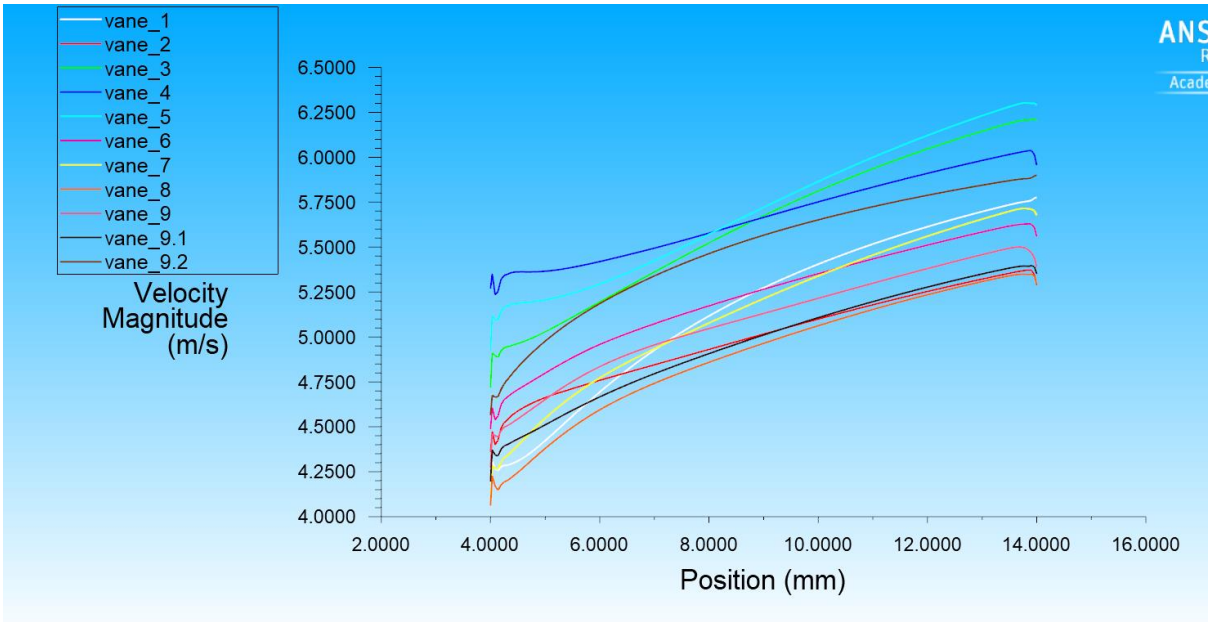

Figure 30: Velocity of each channel

Case 3: 3D nanofluid

Model

The model used in this iteration will be the same microchannel used in Figure 2, but with the addition of a nanofluid. This will form the foundation of this study, with the objective to show that a nanofluid can be correctly added to the Ansys Fluent simulation, considering all the complications that follow. The biggest difference now will be the addition of a UDF, which allows the user to insert any prior defined function into Ansys Fluent as a replacement for any other property. This will be the purpose of the particular models explained by equations 34 to 41

Setup

- 3D case full geometry
- Laminar flow
- SiO_2 as nanofluid
- Heat transfer added 100 W/cm^2
- Reynolds number at inlet of 1 333

All the properties of water and nanofluid were used from the journal entry of Ayoub (in Abdollahi et al., 2017) . However, these were cross-referenced with CES software (CES Edupack, 2014).

Thermophysical properties

The properties of silicon dioxide as a nanofluid will be calculated using the following equations.

Thermal conductivity:

$$k_{eff} = k_{static} + k_{Brownian} \tag{34}$$

$$k_{static} = k_f[\frac{(k_{np} + 2k_f) - 2\phi(k_f - k_{np})}{(k_{np} + 2k_f) + \phi(k_f - k_{np})}] \tag{35}$$

$$k_{Brownian} = 5 \cdot 10^4 \beta \phi \rho_f C_{pf} \sqrt{\frac{KT}{2\rho_{np} d_{np}}} f(T, \phi) \tag{36}$$

where K is the Boltzmann constant (K = 1.3807*10^{-23})

To calculate $f(T, \phi)$, the following equation is used:

$$f(T,\phi) = (2.8217 \cdot 10^{-2}\phi - 3.91123 \cdot 10^{-3})\left(\frac{T}{T_o}\right) + (-3.0669 \cdot 10^{-2}\phi - 3.91123 \cdot 10^{-3}) \quad (37)$$

Specific heat capacity:

$$C_{pnf} = \frac{(1-\varphi)(\rho C_p)_f + \varphi(\rho C_p)_s}{\rho_{nf}} \quad (38)$$

Density:

$$\rho_{nf} = (1-\varphi)\rho_f + \varphi\rho_s \quad (39)$$

Viscosity:

$$\mu_{eff} = \mu_f \cdot \frac{1}{(1 - 34.87\left(\frac{dp}{df}\right)^{-0.3} \cdot \phi^{1.03})} \quad (40)$$

$$df = 0.1\left(\frac{6M}{N\pi\rho_f}\right)^{\frac{1}{3}} \quad (41)$$

The following constants were used to calculate the properties:

Table 4: Properties of nanoparticles at T = 300 K

Thermophysical properties	Water	SiO_2
$\rho\left(\frac{kg}{m^3}\right)$	998.2	2 200
$C_p(\frac{J}{kgK})$	4182	703
$k(\frac{W}{mK})$	0.6	1.2
$\mu(\frac{Ns}{m^2})$	0.001003	0
β	-	$1.9526(100 \cdot \phi)^{-1.4594}$

Results

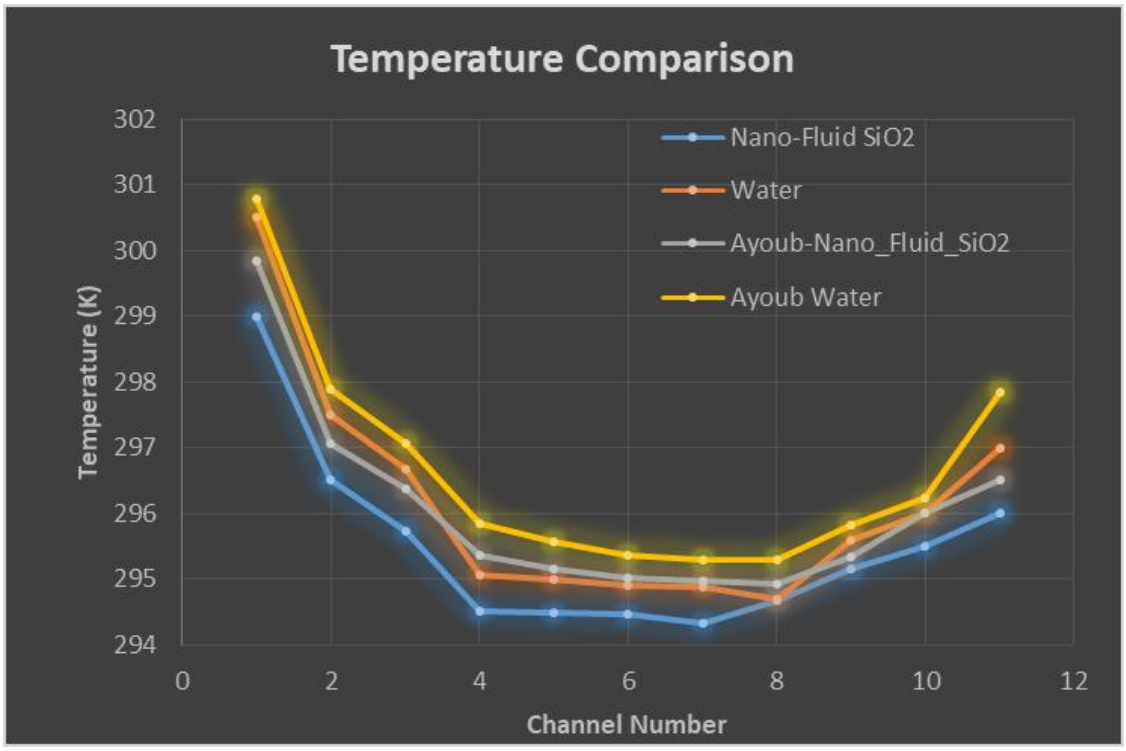

Figure 31: Water and nanofluid temperature: a comparison

From the comparison done above with the temperature of each vane it can be clearly seen that the difference in mesh density did have a big effect on the results. However, this was a first implementation of a 3D model and a nanofluid. The results of this study with both water and nanofluid correlates well with that of previous work. The nanofluid does seem to be correctly implemented as the bigger heat transfer coefficient has allowed more heat transfer to be applied within the fins and thus lowering the temperature.

This validates the concept of nanofluids being used as an optimised heat transfer fluid. This base case simulation will now be the foundation for future analysis. The knowledge gained can now be used to implement more nanofluid models and/or study different parameters. These parameters will then be optimised to find the perfect configuration to ensure the biggest heat transfer coefficient and lowest pressure drop.

Conclusion

From the literature study, it was clear that a gap existed in the field optimisation terms of algorithms for studying nanofluids. Despite a current focus on the implementation of traditional machine learning and optimisation, no real validation has been done. Later, in Section 4.4, the optimisation is shown, as well as the full design study. A base case simulation of silicon dioxide as a nanofluid is presented.

The base case simulation was broken up into three cases. The 2D case was presented to ensure that the correct number of mesh cells was added to each channel of the microchannel heat sink. This was done to confirm that the flow is correctly resolved inside each channel, as this will have adverse effects on the heat transfer. The second case validated the 3D model and mesh. Water was simulated through the microchannel to compare it with previous results. The comparison was done to ensure that the converged solutions are indeed correct. If a simulation is done without validation, the solution can be converged by the system, yet be completely incorrect. For the third simulation, a nanofluid was introduced and the validation done . This is the base case for future simulations and was an exercise to ensure that the knowledge has been established to correctly simulate a nanofluid.

Following these validation results, the design study can be configured, meaning that the current simulation can be duplicated and inputs changed to still give correct results every time. This will allow the user to inspect different inputs at the same time and hopefully gain a greater understanding of the influence of certain inputs. The creation of a design study will be used as data for optimisation.

4.2 DESIGN STUDY

4.2.1 Introduction

In the previous section, successful validation of the numerical results ensured that it can be stated with confidence that the outcome of the simulation has been confirmed and is correct. The next step in the project will be to duplicate the simulation, while changing the material properties to understand what happens to the outcome in terms of heat transfer and pressure drop. This is the beginning of the optimisation step in the project. In order to optimise a system with confidence, sufficient data points are needed. Thus, the design study was developed.

The four different inputs (concentration, diameter, base fluid and nanoparticle) were each varied for four different base fluids and four different nanofluids, and compared with each other to complete a design study with 256 different design points. The number of points is not excessive in terms of optimisation. However, from a simulation point of view, this is a large number of points to simulate individually. These points nonetheless had to be generated to have enough points for optimisation.

The methodology behind simulating all these points was explained in Section 3.4.4.

4.2.2 Results of the design study

Inputs

The inputs of the system are shown in Table 8. Properties of the system are shown Table 9 to confirm what was added to the system. These can be replaced with new materials and fluids, if so desired. In Section 3 the entire setup is explained in order to create a model for future researchers to use. This means that if new nanofluids become available, these can be tested against existing ones. The power of this model therefore lies in enabling anyone to develop a new design study by updating one simple Python script.

Table 5 Inputs of the design study

Inputs	Base fluid	Nanoparticle	Concentration	Diameter
1	Water	Al_2O_3	0,10%	10 nm
2	EG	CuO	0,50%	30 nm
3	W:EG 50:50	SiO_2	1%	60 nm
4	W:EG 60:40	ZnO	5%	100 nm

Table 6 Nanofluid properties

Thermophysical properties	Al_2O_3	CuO	SiO_2	ZnO
$\rho(\frac{kg}{m^3})$	3 970	6 500	2 200	5 600
$C_p(\frac{J}{kg\ K})$	765	535.6	703	495.5
$k(\frac{W}{m\ K})$	40	20	1.2	13
$\mu(\frac{Ns}{m^2})$	0	0	0	0

The nanoparticles tabulated in Table 9 are common in studies done in the field. These were chosen in order to help with the validation of the system against an abundance of data present in literature. These particles will be compared and ranked against each other later in this section. This will provide a better understanding of the influence of the particles for later optimisation.

Table 7: Base fluid properties

Thermophysical properties	Water	EG	W:EG 50:50	W:EG 60:40
$\rho(\frac{kg}{m^3})$	998.2	1 113.2	1 055.7	1 044.2
$C_p(\frac{J}{kg\ K})$	4 182	2 360	3 221.38	3 405
$k(\frac{W}{m\ K})$	0.6	0.258	0.429	0.4632
$\mu(\frac{Ns}{m^2})$	0.001	0.0161	0.0085515	0.0078418

The base fluids described in Table 10 are water and EG, as well as 50:50 and 60:40 combinations of these fluids, respectively. This was done to test the optimisation algorithm further, as the answer will not be that obvious. The particle used has a great influence on the outcome, which will be shown later in the section.

Design points

The design points were generated using a Python script that looped through each of the points in sequence. This meant that all the possible combinations could be calculated. The calculation of the inputs was not as simple as sending the data in Table 8 to Ansys, as Ansys requires the specific material properties of the mixture. The material property models chosen in Section 2.4 of the literature study were then used to calculate the mixture properties. A summary of the equations used is given.

Input equations

Density:

$$\rho_{nf} = (1-\varphi)\rho_f + \varphi\rho_s \tag{42}$$

Specific heat capacity:

$$C_{pnf} = \frac{(1-\varphi)\left(\rho C_p\right)_f + \varphi\left(\rho C_p\right)_s}{\rho_{nf}} \tag{43}$$

Thermal conductivity:

$$k_{eff} = \frac{k_{np} + 2k_f + 2\left(k_{np} - k_f\right)\phi}{k_{np} + 2k_f - \left(k_{np} - k_f\right)\phi} k_f + 5\times 10^4 \beta\phi\rho_p c_p \sqrt{\frac{k_B T}{\rho_p D}} f(T,\phi) \tag{44}$$

Viscosity:

$$\mu_{brownian} = 5\times 10^4 \beta\rho_f \phi_{np} \sqrt{\frac{k_B T}{2\rho_{np} r_{np}}} \left(\left(-134.63 + 1722.3\phi_{np}\right) + \left(0.4705 - 6.04\phi_p\right)T\right) \tag{45}$$

Output equations

Nusselt number:

$$Nu = \frac{q_w D_h}{k(T_{solid} - T_{fluid})} \tag{46}$$

Pressure drop:

$$\Delta P = \frac{1}{2}\rho F Q^2 \tag{47}$$

Each of the inputs listed in Table 8 was then systematically added into the equations above, until the mixture properties were created for each design point. This design point was then exported to Ansys. This was done for each of the design points, and a design study table was developed. The biggest struggle was with the inputs for thermal conductivity. All the other inputs (density, viscosity and specific heat capacity) were constants and could easily be added into Ansys Workbench's parameter system. Thermal conductivity is temperature dependant, however, and changes throughout the system. This type of varying parameter can only be added into Ansys using a UDF, a script using C++ to call parameters inside Ansys and calculate varying properties. A connection through the Ansys parameter system and a UDF was then found through lines of code that had to be run inside Ansys Fluent's text user interface to allow these parameters to be used in the UDF. This method is very difficult as Ansys has no real support for this type of interaction. However, this only has to be done once, making the use of the system less complicated.

Table 8 Workbench input example

Design point	Density	CP	Viscosity	Thermal conductivity	Nanoparticle	Base fluid	Concentration	Diameter
1.	1 001,1718	4 168,450387	0,001	0,60056455	Al2O3	Water	0,001	0,0001
2.	1 013,059	4 115,046891	0,001	0,60285351	Al2O3	Water	0,005	0,0001
3.	1 027,918	4 050,029454	0,001	0,60568333	Al2O3	Water	0,01	0,0001
4.	1146,79	3590,545156	0,001	0,62738028	Al2O3	Water	0,05	0,0001

The example shown in Table 11 is a small part of the design study. As can be seen, the concentration is varied and the rest of the inputs are constant. This is how each possible iteration can be inserted into Ansys.

Ansys will then simulate the given data and produce an output of a Nusselt number and pressure difference. The Nusselt number is calculated in each of the channels, whereas the pressure difference is calculated from the entrance to the exit. The resolved data table in Ansys Workbench can be seen in Figure 32, together with the inputs of the system and the outputs needed to calculate the Nusselt number and pressure drop.

Table of Design Points

	C	D	E	F	G	H	I	J	K	L	M
1	P1 - Density	P2 - CP	P3 - Viscosity	P4 - l1	P5 - l2	P6 - l3	P7 - l4	P8 - t_solid_avg-op	P9 - thermal_conductivity-op	P10 - inlet_p-op	P11 - t_fluid_avg-op
2	kg m^-3	J kg^-1 C^-1	Pa s					K	W m^-1 K^-1	Pa	K
3	1001.2	4168.5	0.001004	0.60057	5038400	0.1323	0.001	336.16464	0.60056916	65968.428	298.49936
4	1001.1718	4168.450387	0.001	0.600573	5038401.721	4.183822	0.001	336.47171	0.6005463	65105.542	298.52117
5	1001.1718	4168.450387	0.001	0.600573	5038401.721	2.41553	0.001	337.02568	0.60055757	63887.119	298.499
6	1001.1718	4168.450387	0.001	0.600573	5038401.721	1.708038	0.001	337.02559	0.60056209	63887.12	298.499
7	1001.1718	4168.450387	0.001	0.600573	5038401.721	1.323041	0.001	337.02553	0.60056455	63887.121	298.499

Figure 32: ANSYS Workbench output

Results

This section will detail the results from the simulation of the entire design study. It examines the performance of some of the nanoparticles and base fluids, as well as the influence that the concentration and diameter have on the outcome. This look at the data will inform us of some of the trends present in the outcome. For the optimisation, an in-depth knowledge of the data is needed to ensure that the outcome is correct.

The first step in the analysis is to determine the values of the different base fluids that are used in the simulations. This is done by plotting the Nusselt number against the pressure drop and separating the different base fluids by colour coding. This indication will show what effect the base fluids have and how close the different sets of data are to each other. It can clearly be seen in Figure 33 that water is a clear, optimal base fluid, as the Nusselt number is the highest and the pressure drop the lowest, making it the optimal fluid for overall heat transfer and performance efficiency. This means that when the optimisation algorithm is run, the expected outcome is for the water to be the only base fluid selected. The performance of EG comes as a surprise as the worst-performing base fluid. The apparent performance of water is justified, with the 60:40 Water:EG mixture delivering the second-best results in terms of pressure drop. However, it does not have near the Nusselt number of water alone.

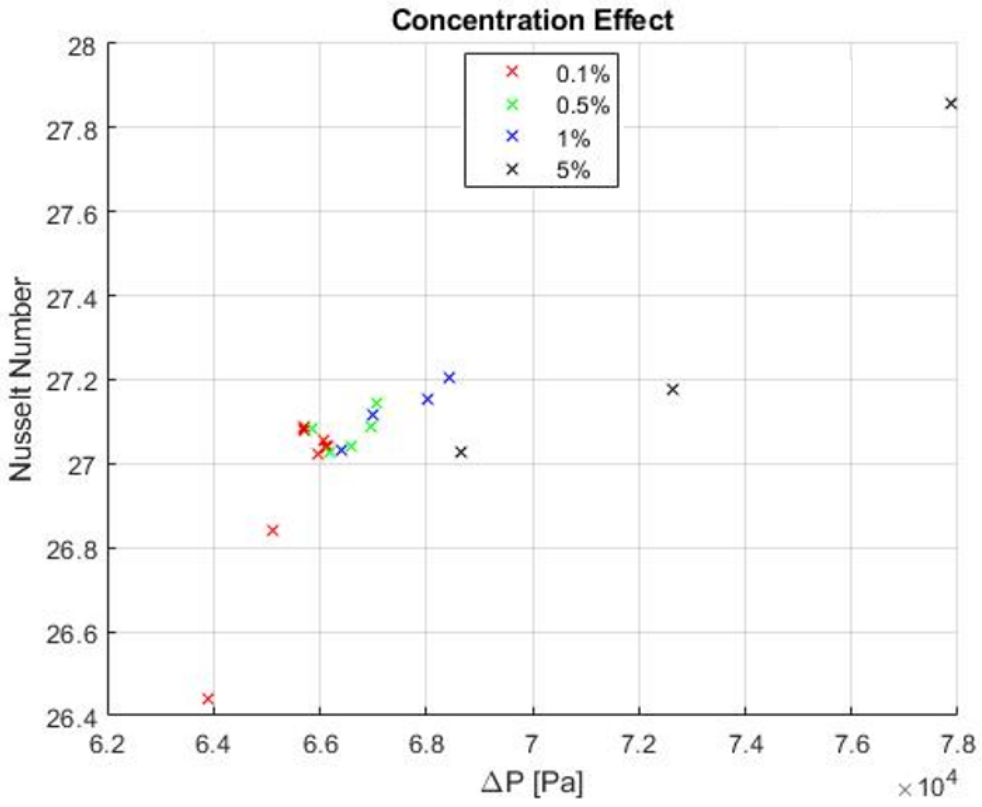

Figure 33: Data comparison

The following step would be to take a closer look at the effect of the concentration and the diameter on the outcome. The selection of only one base fluid, water, clearly shows the relationship with one variable less. Figure 34 shows that the concentration influences the Nusselt number. This influence seems to be exponential, with 5% nanoparticles, yet no clear correlation is seen with other concentration values. This clearly shows why an optimisation algorithm is needed to determine the optimal point in terms of Nusselt number and pressure drop at the same time. As the point with the lowest pressure drop also has the lowest Nusselt number, the optimal point would have the lowest pressure drop and highest Nusselt number. Thus, no conclusion can yet be reached on the influence of the concentration of nanoparticles in the system.

A further examination of the effect of concentration can be seen when all inputs are kept constant and only the concentration is changed. Figure 34 shows what is expected of the concentration. A saturation point is reached where, if the concentration is increased, the Nusselt number will not change. However, the pressure drop increases rapidly as the fluid becomes an entirely wet nanoparticle, losing its fluid properties. The constants and variables used to plot Figure 34 are as follows.

Table 12: Inputs and output of Figure 34

Inputs			Output
Base fluid	Nanoparticle	Diameter	Concentration
water	SiO_2	100 nm	variable

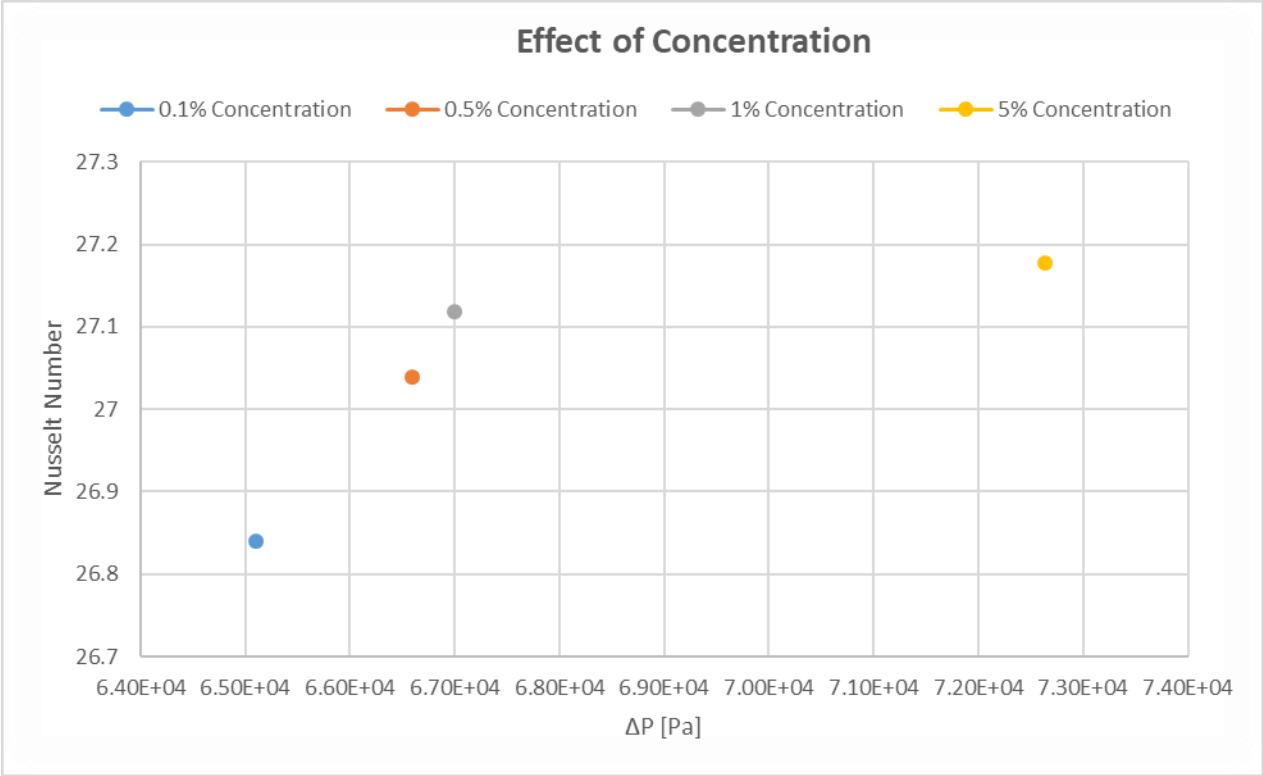

Figure 34: Concentration effect on heat transfer

The 5% concentration of nanoparticles has the highest Nusselt number, but an extremely high pressure drop, showing that this many nanoparticles in the system will have a negative effect on pumping efficiency. The 1% of nanoparticle concentration offers a far better solution with an acceptable pressure drop and a Nusselt number extremely close to 5%. Figure 34 illustrated the effect of the concentration on both output variables, the Nusselt number and pressure drop. However, a better comparison would be to have the dependant variable as one of the x or y axis functions. The following graphs depict some interesting discoveries. The concentration has a positive effect on the Nusselt number and pressure drop. If optimisation must be done on these outcomes, a sensitivity analysis will determine the outcome. It can clearly be seen that the influence on the pressure drop is much more drastic than that of the Nusselt number, meaning that a small drop in Nusselt number ensures a considerable drop in pressure. A small compromise in heat transfer gives a big gain in pumping efficiency.

Table 9: Inputs for figures 35 and 36

Inputs			Output
Base fluid	Nanoparticle	Diameter	Concentration
Water	varying	100 nm	varying

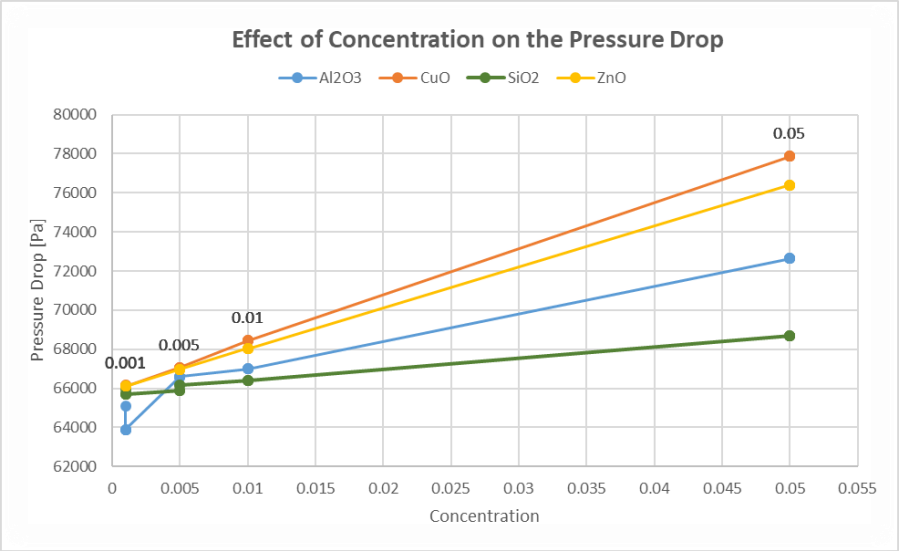

Figure 35: Comparison of nanoparticles and the influence of concentration on pressure drop

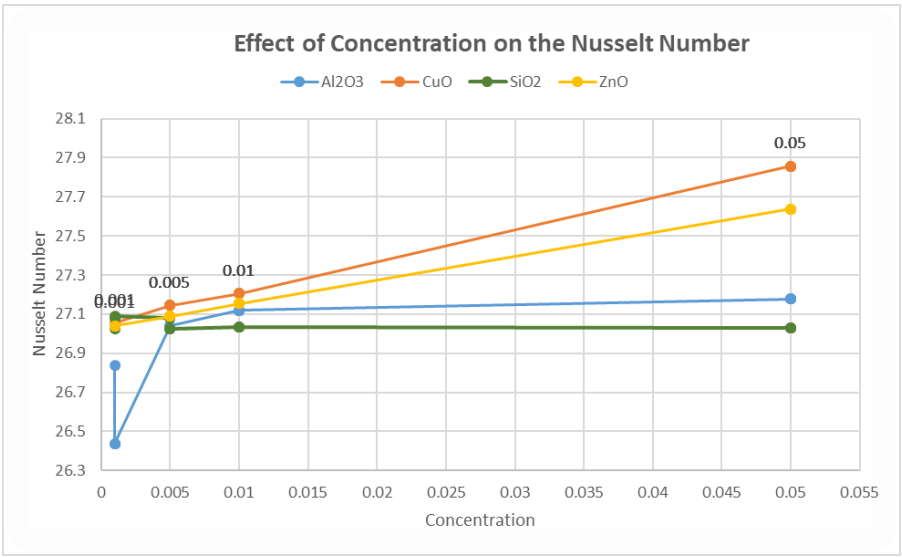

Figure 36: Comparison of nanoparticles and the influence of concentration on the Nusselt number

The following analysis will be done on the effect of the nanoparticles on the Nusselt number and pressure drop. This will determine if any relationship is apparent.

Table 10: Inputs and outputs for Figure 37

Inputs			Output
Base fluid	Nanoparticle	Diameter	Concentration
Water	Variable	100 nm	1%

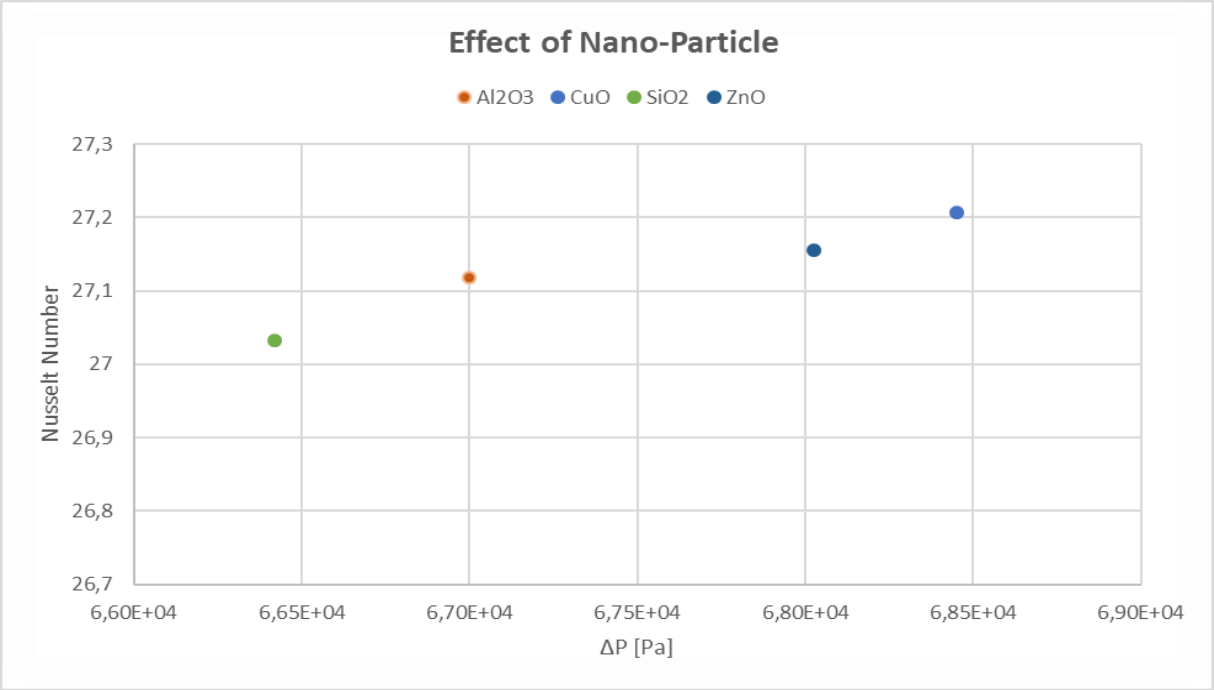

Figure 37: Comparison of the nanoparticles' effect

From Figure 37, it is clear that the influence on the Nusselt number is small. However, the pressure drop change is extensive. This means that the zinc oxide nanoparticle performs the worst with the biggest pressure drop. As the difference between silicon dioxide and zinc oxide is only point two, this clearly shows that after the optimisation, the expected results would be that the performance of the silicon dioxide could be optimal. The small decrease in heat transfer offers a big advantage in pressure drop. This sensitivity between outputs is vital knowledge gained for later optimisation outcomes.

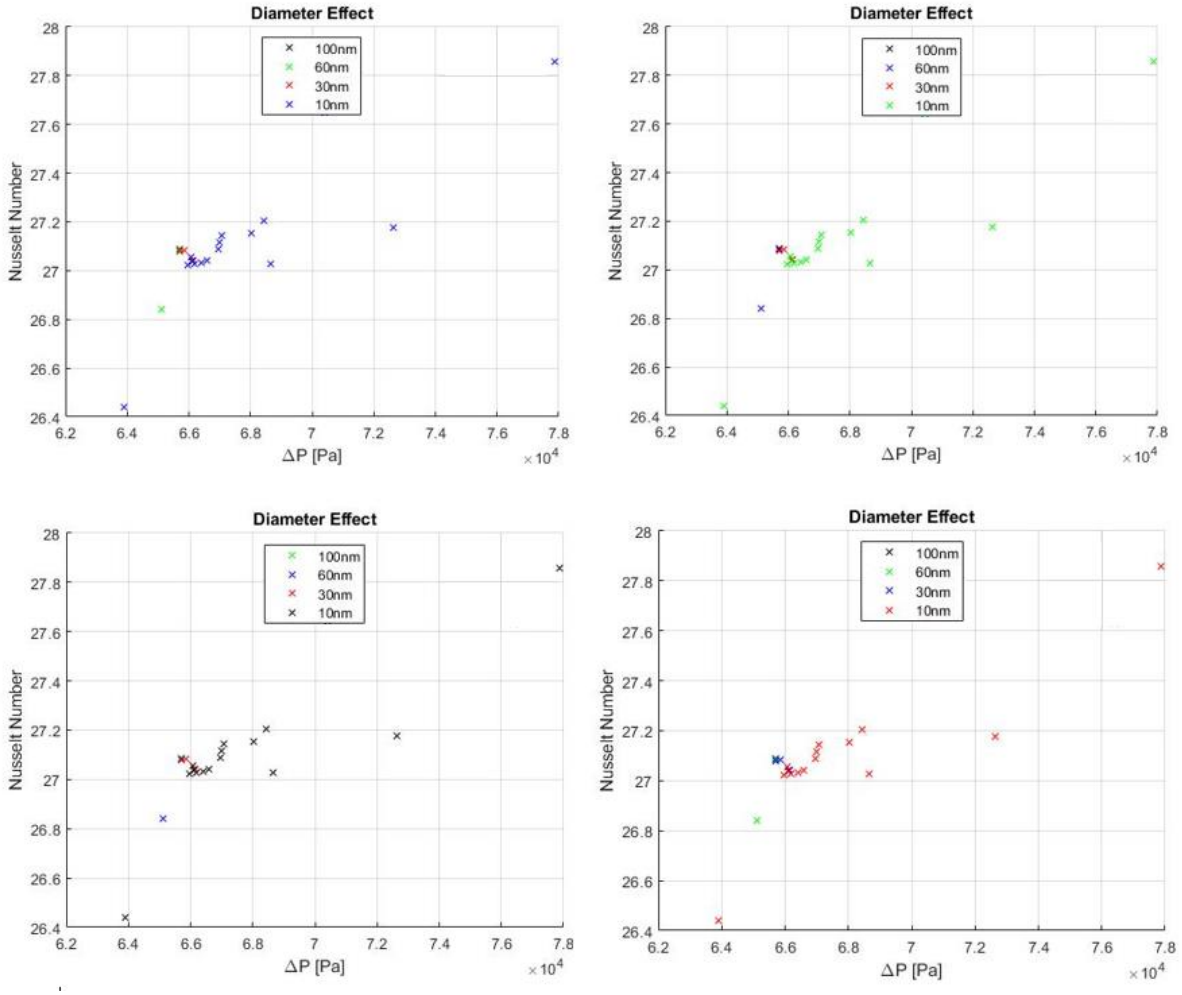

Figure 8: Effect of diameter on the Nusselt number and pressure drop

The effect of the diameter on the Nusselt number and pressure drop in water as the base fluid was then compared. No correlation appeared to exist between the two sets of data. In Figure 38, the colour order was changed to show that whatever colour was plotted last was the one that would be seen. It then became evident that the colour order in which the data points were plotted changed the outcome of the graph. This meant that several points were on precisely the same position, which made it appear as if the diameter had little to no influence on the outcome, as different points were plotted on or near the same point on the graph. The inputs for the following graphs are as follows:

Table 11: Inputs and output for Figure 38

	Inputs		Output
Base fluid	Nanoparticle	Diameter	Concentration
Water	variable	variable	variable

This conclusion that the diameter had an extremely small effect on the data was confirmed by raw data from Ansys Fluent. A filter was applied so that all the input parameters were constant except for diameter. The outcomes of the Nusselt number and pressure drop are almost constant for all four diameters, as shown in Table 15, where the inputs and outputs are listed. The variation in Nusselt number is too small to be discernible on a standard plot.

Table 12: Diameter effect on Nusselt number

Design point	Nanoparticle	Base fluid	Concentration	Diameter	Nusselt number	Pressure drop
1.	Al2O3	Water	0,001	1,00E-08	26,83947553	65105,542
2.	Al2O3	Water	0,001	3,00E-08	26,4376135	63887,119
3.	Al2O3	Water	0,001	6,00E-08	26,43747628	63887,12
4.	Al2O3	Water	0,001	1,00E-07	26,43740916	63887,121

From Table 16, it is evident that the lowest nanoparticle diameter had the highest pressure drop. This is due to the higher velocity in the channels for the smaller diameter. The higher Nusselt number for the lower diameter comes from the relation to the added Brownian motion relative surface area. The larger surface area of the smaller particles enhances heat transfer and allows for a larger Nusselt number.

The fluid flow rate and pressure drop, as well as the fluid velocity, are listed in Table 17 to demonstrate the higher pressure drop phenomenon of the smaller diameter. This is due to the viscosity increasing with a smaller diameter, as the diameter is in the denominator of the viscosity formulation seen in the beginning of Section 4.2.2.

Table 13: Influence of the diameter on velocity and flow rate

Diameter	Nanoparticle	Base fluid	Concentration	Velocity (m/s)	Flow rate (m^3/s)	Pressure drop (Pa)
10 nm	Al_2O_3	Water	0,001	5.9	4.41e-6	65105,542
30 nm	Al_2O_3	Water	0,001	5.8567	4.32e-6	63887,119
60 nm	Al_2O_3	Water	0,001	5.5618	4.16e-6	63887,12
100 nm	Al_2O_3	Water	0,001	5.4536	4.15e-6	63887,121

In conclusion, the effect of the diameter on the system is small with only some discernible effects on flow rate and velocity. The lower the diameter, the larger the specific heat removal area, inducing a larger pressure drop and a larger Nusselt number. The optimal can, however, not be determined as some specific regain (feedback) between the diameters can exist where the Nusselt number remains high in the presence of a pressure drop. This is another indication that algorithms and optimisation techniques are needed for greater clarification. Figures 39 and 40 show the same relationship as in Table 17 where the diameters' influence on the outcome is extremely small.

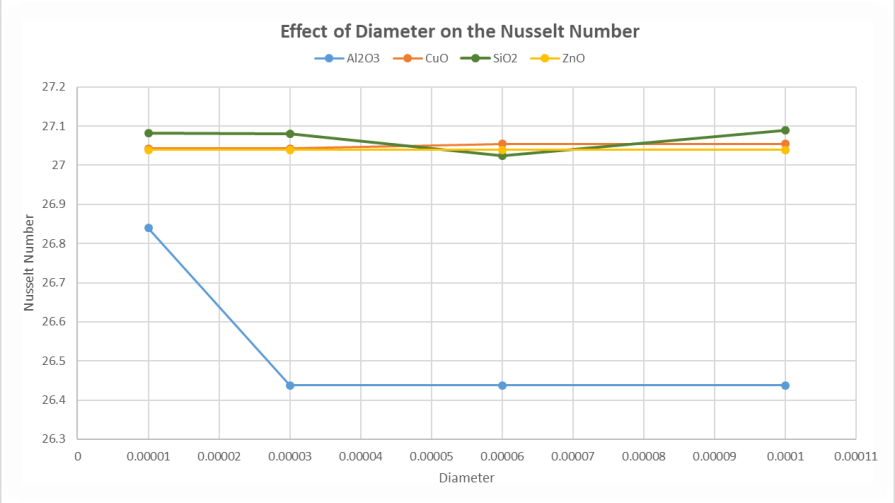

Figure 39: Comparison of the nanoparticle and the influence of diameter on the Nusselt number

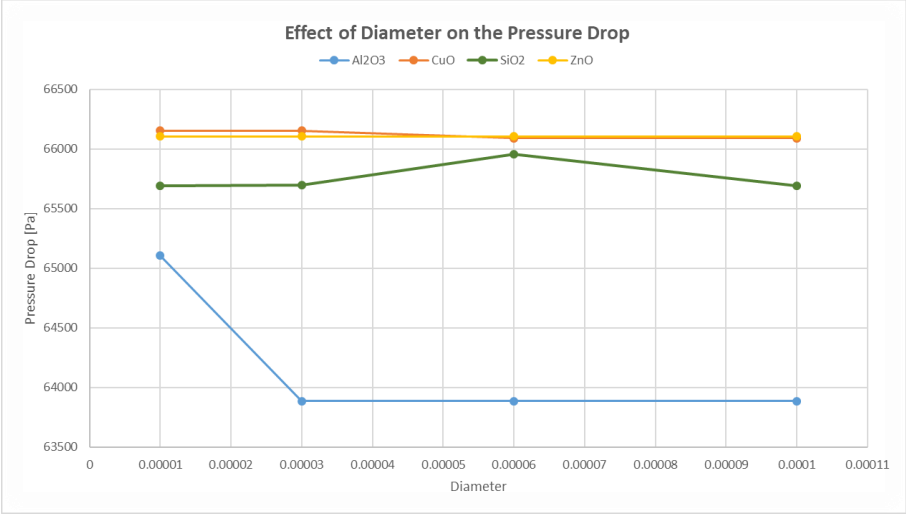

Figure 40: Comparison of the nanoparticle and the influence of diameter on pressure drop

4.2.3 Conclusion

In Section 4.1 the validation of the Ansys Fluent simulation model was gained and confirmed. The model it could be duplicated with confidence in Section 4.2 to create the design study. This design study was successful in creating sufficient design points that can be analysed and optimised. Before the optimisation could be done, the design study had to be carefully analysed. This then showed trends and possible answers. Section 4.2.2 discussed some of the relations discovered. These relations indicate possible optimisation flaws if the algorithm gives an answer that is not predicted. The power of analysing the data before optimisation is incredible and must be done.

The following conclusions could be drawn from the data: For the diameter, no connection was seen between the outcome of the Nusselt number and pressure drop. The influence on the outputs was so small that no conclusion could be drawn. However, it does seem that the lower the diameter, the larger the specific heat capacity , as the velocity and flow rate are increased, theoretically leading to better heat transfer.

The conclusion regarding concentration is that the concentration has an almost linear effect on Nusselt number and pressure drop with a saturation point reached above 1% for the nanoparticle. This leads to the knowledge that an excess of particles increases pressure drop exponentially , which has a detrimental effect on the pumping efficiency of the system.

As far as nanoparticle composition is concerned, silicon dioxide yields the best outcome due to the lower density of the particle. The decrease in Nusselt number with silicon dioxide compared to that of the zinc oxide is small enough, but the decrease in pressure drop is extensive and leaves silicon dioxide as the preferred option.

4.3 OPTIMISATION

4.3.1 Introduction

The design study was successfully created and simulated in Ansys Fluent. The outputs and corresponding inputs have been exported to Excel and MATLAB for further analysis. The base analysis was done in Section 4.2.2, which highlighted some functions and relations between the inputs and outputs. This will help to ensure that the design of further optimisation is done correctly and with confidence. The optimisation algorithm will work in the following steps:

1. Regression of the design study
    a. This regression model will devise a function to classify and characterise all the data in the design study. One function will be for the Nusselt number and one for the pressure drop. The two functions will then be used to maximise the Nusselt number function and minimise the pressure drop function.
2. Optimisation of the regression functions
    b. Now that the functions have been classified, the functions can be optimised. This will allow for faster optimisation.

The chosen method for the regression of the data was an radial basis function (RBF). The power of this function lies in the number of coefficients it produces. This method is suitable when users have gone to great lengths to collect precise data. It would be counterproductive to lose accuracy by employing a function that only approximates the data. The RBF functions iterate perfectly through every given data point.

4.3.2 Regression model of numerical results

A radial basis function translates a radially symmetric function that is linearly combined to approximate an unknown function, so that the following can be stated:

$$\varphi(X) = \varphi(\|X\|) \tag{48}$$

Any function that satisfies Equation 48 can be classified as a radial function. The computing of an RBF uses, in most parts, the reconstruction of an unknown function for known data. This satisfies the data format of the current study as well; the design study supplied the known data from Ansys Fluent with known inputs and outputs. An RBF can be used as a collection $\{\varphi_k\}_k$ that forms a function of interest. Approximates of functions are done in this manner by summation of the RBF at each data point.

The general form of an RBF can be seen in Equation 49.

$$s(x) = \{\sum\nolimits_{\zeta \epsilon \Xi} \lambda_\zeta \|\cdot - \zeta\| | \lambda_\zeta \in R\} \tag{49}$$

where ζ refers to the data sites, λ_ζ are the real coefficients and $\|\cdot - \zeta\|$is the Euclidean distance from the origin. In Equation 49, the radial basis function is simply described as $\varphi(r) = r$.

The following RBF can be used to test the data. Each data set can be different. For the model created to be universal with any nanofluid and any iteration of the designed inputs, a code was written that tests each different RBF and determines the best fit. Most RBFs also include the use of a shape factor that influences the scale of the input to better fit the data.

Table 18: Radial basis functions

RBF	$\varphi(r)$
Linear	εr
Cubic	$(\varepsilon r)^3$
Thin plate	$(\varepsilon r)^2 \log(\varepsilon r)$
Quadratic	$1 + (\varepsilon r)^2$
Multiquadric	$\sqrt{1 + (\varepsilon r)^2}$
Inverse multiquadric	$\frac{1}{\sqrt{1 + (\varepsilon r)^2}}$
Inverse quadric	$\frac{1}{1 + (\varepsilon r)^2}$
Gauss	$e^{-(\varepsilon r)^2}$

Shape factors are notoriously difficult to determine as they are strongly influenced by the specific data set. Most shape factors are determined by trial and error, but, since the model has to determine the shape factor for each new data set given, the shape factor will be determined once for the data set using another script. This script will change the shape factor and determine the quality of fit from the error of the output from the function for a given input. The same is done with the RBF itself. All the functions listed in Table 18 will be implemented and the best one chosen for the current set. This ensures that any new data generated by Ansys Fluent can still be optimised. This adds value to the model to ensure its further use without alterations being needed.

The influence of a shape function can have a great effect on the accuracy of a model, as can be seen in Figure 41. The function still transverses the data point at the top (1, 0), but changes shape as the shape function changes. The effect of a shape function is mostly seen by the changes it makes between data points as RBFs transverse all data points precisely.

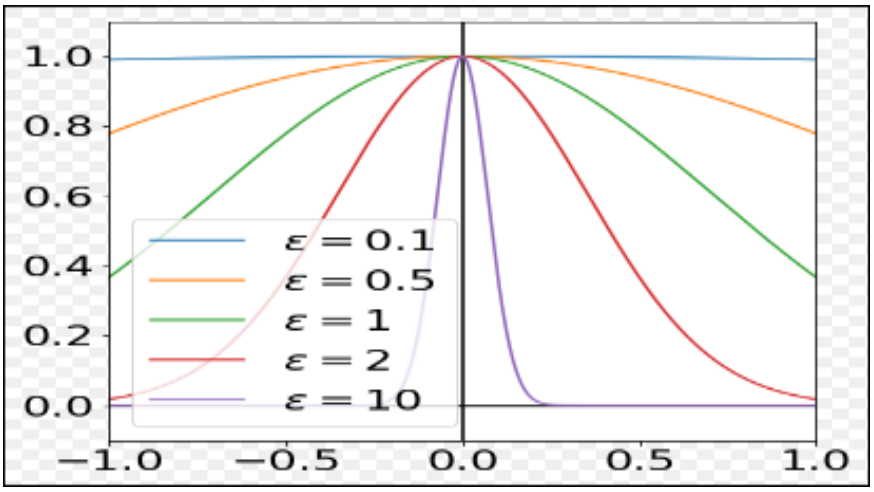

Figure 41: Influence of the shape function

Error behaviour in radial basis functions are local and are in terms of the distance from the centre discrete variables. For some of the infinitely smooth RBFs (i.e. Gaussian and inversely multiquadric functions), the interpolation error converges at an exponential rate. The distance to the centres can be calculated with the following equation:

$$h \coloneqq h(X, \Omega) \coloneqq min\|x - y\| \tag{50}$$

by using the discrete set of centres X in respect to the chosen working domain Ω.

One of the reasons for employing RBFs as a regression technique is that RBFs seems to be immune to the proverbial “curse of dimensionality”. The “curse of dimensionality” was encountered in this project as well, where four inputs and one output was present. With the output being either the Nusselt number or the pressure drop, and the inputs being the concentration, diameter, base fluid and nanoparticle, the only way to show this equation and the effect of the implemented RBF on the data is showing a 3D case of the data. Both cases show how an RBF would interpret the data if fewer inputs were chosen. This is shown in figures 42 and 43. A more informative 5D solution cannot be represented visually.

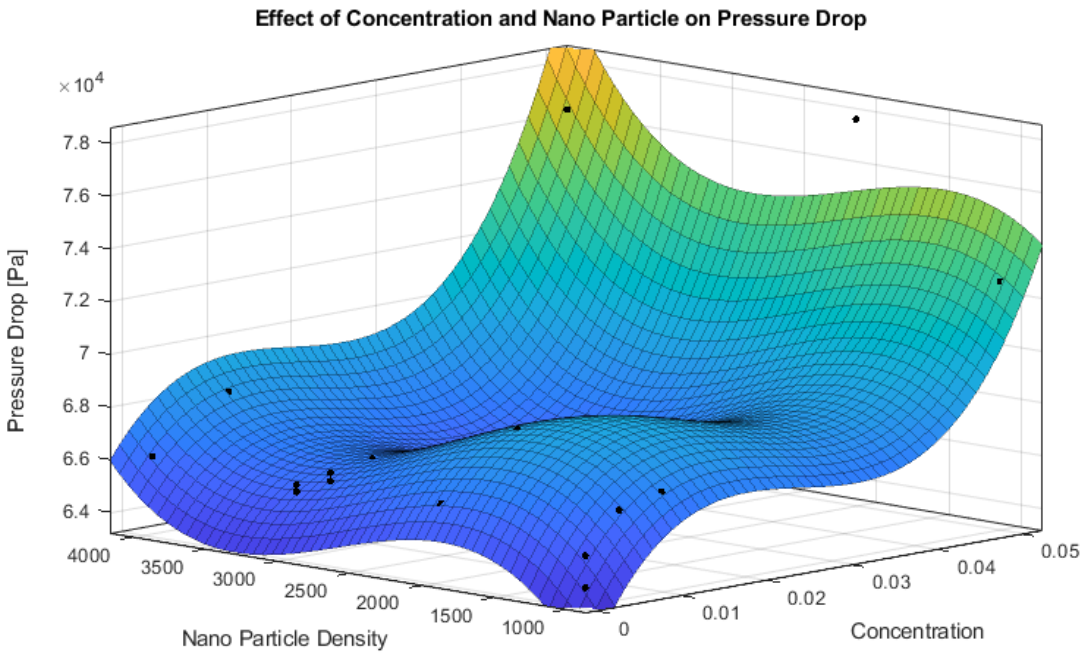

Figure 42: The RBF of the pressure influence

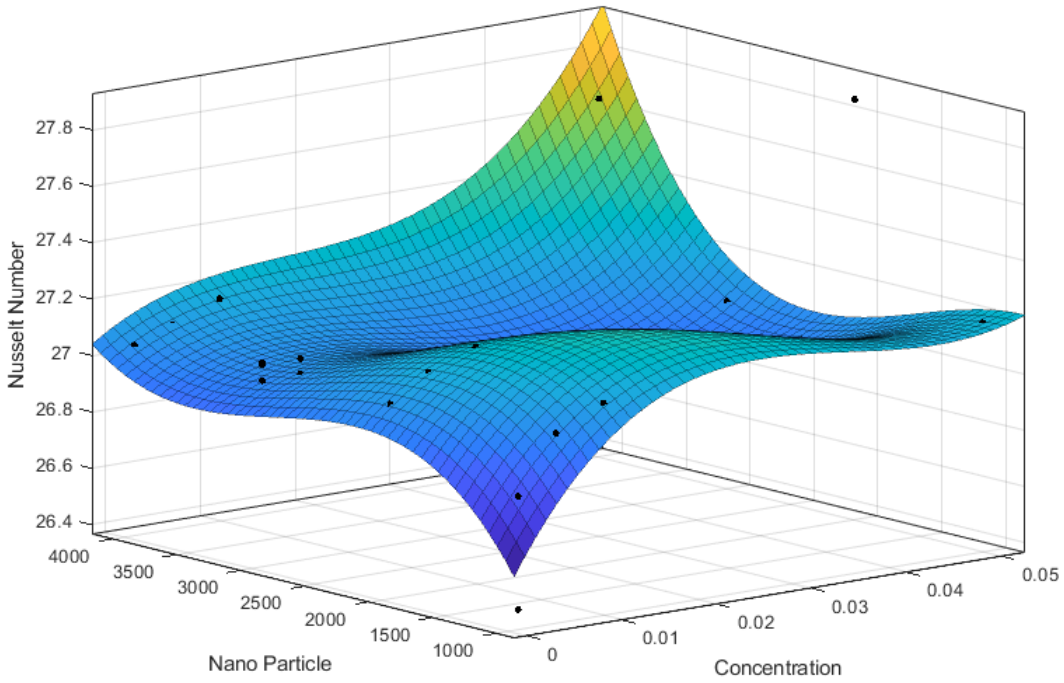

Figure 9: RBF of the influence of the Nusselt number

4.3.3 Optimisation analysis and results

The Ansys simulation was configured and validated with other numerical results. The model was then duplicated into a design study. The material properties were varied and a design study was created. The design points gave different iterations of the four inputs selected. Two outputs were made to determine the heat transfer and pressure drop to be able to quantify the performance of each design point. The design study was characterised, and a RBF created. These RBFs can now be used in an optimisation algorithm. The functions are created so that no further simulation needs to be done, which is incredibly time consuming. The simulations have been done and further simulations need to be avoided if possible.

An in-house optimisation code was used to perform the multi-objective optimisation. The idea was that heat transfer had to be maximised and pressure drop minimised at the same time to determine a combination of inputs that have the best heat transfer for the lowest pressure drop.

The multi-objective optimisation problem is based on the fact that there are conflicting objectives: pressure drop and heat transfer.

The algorithm used was a fast and elitist multi-objective genetic algorithm, the second-generation non-dominated sorting genetic algorithm (NGSA-2), which not only gives one optimal solution, but a Pareto optimal solution. This is a front of solutions, each showing an optimal point for the system. This is due to the multi-objectives of the algorithm. However, it is a usable feature that the user can manipulate it to suit his needs and still have an optimal result.

The NSGAs have, in the past, been criticised for having the following problems:

- A large computational complexity: It has a complexity of $O(MN^3)$, with M being the number of objectives and N the size of the current population. This makes a large population size non-usable if time constraints are applied.
- No elitism in the approach: Elitism is where the best of the child and parent is kept. Elitism has been seen to have adverse effects on the speed and convergence rate of genetic algorithms. It will also help if the loose prevention of optimal answers is obtained (Zitzler et al., 2000).
- Sharing parameters have to be calculated and specified: This parameter is used to ensure that variety in a population is big enough to cover all the optimal answers. However, this also takes up computational time (Fonseca and Fleming, 1998).

The solution for the three listed problems with a NSGA was fixed and a new method proposed by Deb et al. (2002). This method was adopted and used for the University's in-house optimisation code. The solution to the three suggested problems listed above was solved as follows:

- The computational complexity was reduced from n^3 to n^2 dependency, where n represents the population size. This was achieved by calculating a domination count with each front. After each front is calculated, the domination count is lowered and the front is stored in another list. This is continued for each front. This means that the domination count can at most be n-1, ensuring that each solution only gets visited n-1 times. Computing solutions are achieved faster and solutions are not revisited more than is needed to reduce computational complexity.
- Elitism is introduced by comparing the current front with previously optimal solutions. This fairly simple approach adds a lot of value and increases the confidence value by ensuring that optimal answers are not lost.
- The sharing function was replaced with a crowded comparison approach. A density estimation technique is added to determine the exact state of the diversity in the system. The overall crowding factor is calculated by the summation of individual distances to each objective. This is then used as a crowded comparison operator calculated at each front that drives the selection process to diversify.

Once the algorithm has been chosen, and the power and efficiency explained, the code can be run through the data. Both objectives are specified and the number of input parameters given. The code offers the option of selecting the number of generations and population size. These inputs differ from simulation to simulation, as do data specifics. Generations are used as children mutated from the parents, where population shows the number of different entries that are tried and tested in each generation. It was seen through some trial and error that a generation count of 200 and a population count of 2 000 offered the best results. This was due to the data set being densely packed so that large variation was not needed, however, the densely packed data needed enhanced precision as the values were small and close to one another.

As stated previously, the praetor front is generated with NSGA-II, giving multiple answers and ensuring the user can choose a selection that will work practically and experimentally. The NSGA-II inputs are tabulated in Table 19. The functions that were given as two objective functions were created and explained in Section 4.3.2 to ensure computational time is lowered as much as possible. No re-simulation was needed.

To validate the RBF functions and NSGA-II code, the outcome of the algorithm was fed back to Ansys to ensure that the generated Nusselt number and pressure drop were still correct.

Table 19: NSGA-II inputs

Objective functions	Minimise	Maximise	Population	Generations
Nusselt number RBF		Maximise the heat transfer	2 000	200
Pressure drop RBF	Minimise the pressure drop			

The result of NSGA-II is published in a text document showing the results. The results were analysed and compared to some of the predictions made in Section 4.2.2 when the results of the design study were post-processed. The predictions made are indicated below and seen in the results. This further validated the optimisation and RBFs.

Influence of concentration

The concentration effect could be seen in Figure 35 and 36 where an increase in the concentration resulted in a less efficient system with substantial heat transfer, but also a big pressure drop. As predicted, the sensitivity analysis deduced that a lower concentration would offer a very small heat transfer reduction, but a great pressure loss reduction. Weaker concentrations would then deliver better results, as shown by the high pressure drop values at the beginning of Table 20, and lowering pressure drops as the concentration goes down, showing that a 1% nanoparticle concentration might be optimal.

Influence of diameter

As predicted, diameter had a very small effect on the data, and the prediction was that the optimisation would have every one of the diameter values as an option. This can be clearly seen in the results of Table 20. All diameter values are present as they have no discernible influence. This was again validated by the findings of Ayoub (in Abdollahi et al., 2017).

Influence of base fluid

It was predicted that water would be the optimal base fluid, as its Nusselt number was the highest and its pressure drop the lowest. This is confirmed in Table 20 as water is the only base fluid that has been identified in optimal solutions.

Influence of nanoparticles

The influence of the nanoparticle is very complex and shows that copper oxide is the optimal nanoparticle in many instances, with silicon dioxide being a preferred choice in other instances, as reflected in Table 20 (data entry 6). It is concluded that this is the optimal result of the entire design study.

Table 20 (data entry 6) is of particular interest as it presents a very low pressure drop and a relatively high heat transfer rate with a Nusselt number of 28.002. The difference between this entry and a copper oxide entry in pressure drop is just over 1 000 Pa.

Table 14: NSGA-II results

Design point	Concentration	Base fluid	Nanoparticle	Diameter	Nusselt number	Pressure drop
1.	0.0500	Water	CuO	0.0000001	28.879	77 875.192
2.	0.0500	Water	CuO	9.86E-08	28.879	77 875.191
3.	0.0500	Water	CuO	9.14E-08	28.878	77 875.190
4.	0.0500	Water	CuO	7.57E-08	28.878	77 875.190
5.	0.0500	Water	CuO	4.43E-08	28.876	77 875.190
6.	0.0010	Water	SiO2	0.0000001	28.002	65 813.352
7.	0.0049	Water	CuO	6.29E-08	26.148	65 813.346
8.	0.0049	Water	CuO	6.14E-08	26.148	65 813.324
9.	0.0049	Water	CuO	0.00000006	26.148	65 813.305
10.	0.0049	Water	CuO	5.86E-08	26.148	65 813.289
11.	0.0049	Water	CuO	5.71E-08	26.148	65 813.270
12.	0.0049	Water	CuO	5.57E-08	26.148	65 813.257
13.	0.0049	Water	CuO	5.43E-08	26.148	65 813.232
14.	0.0049	Water	CuO	5.29E-08	26.148	65 813.216
15.	0.0049	Water	CuO	5.14E-08	26.148	65 813.203
16.	0.0049	Water	CuO	0.00000005	26.148	65 813.181
17.	0.0049	Water	CuO	4.86E-08	26.148	65 813.165
18.	0.0049	Water	CuO	4.71E-08	26.148	65 813.145
19.	0.0049	Water	CuO	4.57E-08	26.148	65 813.127

4.3.4 Conclusion

This section focused on the validation of the numerical results, as well as the setup of the design study and its optimisation. The data was analysed in the design study to determine some preliminary results, and these predictions were seen in the final optimised data using a genetic algorithm. This is of great importance as it shows that the algorithm works, as well as the characterising RBFs used to define the data. All the data in Table 20 can be used as an optimal point from the Pareto distribution that a fast and elitist multi-objective genetic algorithm produces. However, upon further inspection, the most optimal point was identified. Water was the preferred base fluid option in the design study section. This was confirmed in Table 20. The diameter selection did not have a very big influence on the data. The best nanoparticle was seen to be silicon dioxide, as it offered a lower density, inducing a much lower pressure drop than copper oxide.

Table 21 tabulates the inputs and outputs of the design study, and gives the optimal point.

Table 15 Design study inputs and outputs

Inputs	Base fluid	Nanoparticle	Concentration	Diameter
1.	Water	Al_2O_3	0,10%	10n m
2.	EG	CuO	0,50%	30 nm
3.	W:EG 50:50	SiO_2	1%	60 nm
4.	W:EG 60:40	ZnO	5%	100 nm

The optimal solution can be identified as follows:

Table 16: Optimal solution of the design study

Inputs	Base fluid	Nanoparticle	Concentration	Diameter
1	Water	SiO_2	1%	Any in range

CHAPTER 5: CONCLUSION

The study set out to model and optimise nanofluids in microchannels. This was done by gaining knowledge on the theory of fluid flow in microchannels and the material behaviour models used to characterise these nanoparticles in fluids. The geometry was selected to be a small microchannel that would fit onto a computer chip. The models of material property selection that define the behaviour of nanofluids were selected in order to have enough parameters that could be changed for later optimisation. The results of the Ansys Fluent simulation were validated with numerical and experimental work. This simulation was duplicated to ensure that the flow regime would stay the same, while the material properties were changed in relation to different inputs. The inputs that were changed were the base fluid, nanoparticle material, concentration of nanoparticle in the base fluid and nanoparticle diameter. A design study of 256 different combinations of those inputs were created to have enough data points for simulation. A model was developed that automated the simulation to enable any researcher to repeat the analysis with new data following a few simple steps. This allowed for the manipulation of any inputs into any of the selected parameters and gauging the usefulness of such new inputs against the existing data. The database can therefore be continually used and/or expanded. This adds functionality in that the current data is not the only data that can be used, new inputs can generate new data for optimisation, thus adding continuation to the study. The model that was developed has a functionality that automates all the steps to ensure ease of usability. This design study was then used to determine the effects of certain parameters on the outcome.

The design study data was characterised with RBFs to precisely traverse all data points. Two target parameters were identified to supply the genetic algorithm with objective functions: one to be maximised (the Nusselt number) and one to be minimised (the pressure drop). This would yield an optimal answer, where the heat transfer and pumping efficiency is maximised. This algorithm was run using the generated Ansys data.

The project was successful in that it was proven that the model that was developed and refined works correctly. The final NSGA-II results and the optimal point were fed back into Ansys Fluent for verification and validation to ensure that the RBF and the genetic algorithm work and are accurate. There was a 1 to 3% error in the results due to rounding errors made in the transfer from Ansys Workbench to MATLAB.

Table 17: Optimal point

Inputs	Base fluid	Nanoparticle	Concentration	Diameter
1	Water	SiO_2	1%	Any in range

CHAPTER 6: RECOMMENDATIONS

The result of the study was, indeed, what was expected. The optimal point was found and a model was developed that any user could use by altering the inputs in order to generate and resolve another study. The next steps in the study would be to add another element of automation to the model. The current optimisation algorithm uses an RBF that is characterised by the data to determine the optimal point. If a point is selected between the initial given points of interest, for instance, a concentration of 0.003, the RBF could still be used.

The best option would be to include a step where, if an unknown point is requested (a point that was not resolved before), this new input data will be sent to Ansys Fluent and to resolve that point of interest again. This will increase the confidence in the outcome. However, for this to be implemented, the current model still has to be developed and tested.

This new addition of active feedback from the optimisation algorithm would ensure that all optimal points are resolved in Ansys Fluent and that the optimal option is perfect. It was seen that the current RBF method works well and gives the desired results.

CHAPTER 7: REFERENCES

Abdallah, S. R. *et al.* (2018) 'Experimental investigation on the effect of using nano fluid (Al2O3-Water) on the performance of PV/T system', *Thermal Science and Engineering Progress*, 7(April), pp. 1–7. doi: 10.1016/j.tsep.2018.04.016.

Abdollahi, A. *et al.* (2017) 'Fluid flow and heat transfer of nanofluids in microchannel heat sink with V-type inlet/outlet arrangement', *Alexandria Engineering Journal*. Faculty of Engineering, Alexandria University, 56(1), pp. 161–170. doi: 10.1016/j.aej.2016.09.019.

Adio, S. A. (2015) *Experimental Investigation and Mathematical Modelling of Thermophysical Properties of Ethylene Glycol and Glycerol-Based Nanofluids*. University of Pretoria.

Amani, M. *et al.* (2017) 'Modeling and optimization of thermal conductivity and viscosity of MnFe2O4 nanofluid under magnetic field using an ANN', *Scientific Reports*. Springer US, 7(1), pp. 1–13. doi: 10.1038/s41598-017-17444-5.

Ansys, I. (2013) 'Ansys Fluent Theory Guide', *ANSYS Inc., USA*, 15317(November), pp. 724–746.

Asinari, P. *et al.* (2018) 'Effect of interfacial thermal resistance and nanolayer on estimates of effective thermal conductivity of nanofluids', *Case Studies in Thermal Engineering*, 12(June), pp. 454–461. doi: 10.1016/j.csite.2018.06.005.

Azimi, S. S. and Kalbasi, M. (2014) 'Numerical study of dynamic thermal conductivity of nanofluid in the forced convective heat transfer', *Applied Mathematical Modelling*. Elsevier Inc., 38(4), pp. 1373–1384. doi: 10.1016/j.apm.2013.08.027.

Azizi, Z., Alamdari, A. and Malayeri, M. R. (2015) 'Convective heat transfer of Cu-water nanofluid in a cylindrical microchannel heat sink', *Energy Conversion and Management*. Elsevier Ltd, 101, pp. 515–524. doi: 10.1016/j.enconman.2015.05.073.

Baba, M. S., Raju, A. V. S. R. and Rao, M. B. (2018) 'Heat transfer enhancement and pressure drop of Fe3O4 -water nanofluid in a double tube counter flow heat exchanger with internal longitudinal fins', *Case Studies in Thermal Engineering*. Elsevier Ltd, 12(August), pp. 600–607. doi: 10.1016/j.csite.2018.08.001.

Breuer, M., Jovičić, N. and Mazaev, K. (2003) 'Comparison of DES, RANS and LES for the separated flow around a flat plate at high incidence', *International Journal for Numerical Methods in Fluids*, 41(4), pp. 357–388. doi: 10.1002/fld.445.

Brinker, C.J. and G.W. Scherer, Sol-Gel Science: The Physics and Chemistry of Sol-Gel Processing, Academic Press, San Diego, CA, 1990.

Buhmann, M. D. and Levesley, J. (2004) 'Radial Basis Functions: Theory and Implementations', *Mathematics of Computation*, 73(247), pp. 1578–1581. doi: 10.1017/CBO9780511543241.

Cao, H. *et al.* (2018) 'Flow and heat transfer behaviour of nanofluids in microchannels', *Progress in Natural Science: Materials International*, 28(2), pp. 225–234. doi: 10.1016/j.pnsc.2018.03.005.

CES EduPack software, Granta Design Limited, Cambridge, UK, 2009.

Chen, H. *et al.* (2007) 'Rheological behaviour of ethylene glycol based titania nanofluids', *Chemical Physics Letters*. North-Holland, 444(4–6), pp. 333–337. doi: 10.1016/J.CPLETT.2007.07.046.

Chein, R. and Chen, J. (2009) 'Numerical study of the inlet/outlet arrangement effect on microchannel heat sink performance', *International Journal of Thermal Sciences*. Elsevier Masson SAS, 48(8), pp. 1627–1638. doi: 10.1016/j.ijthermalsci.2008.12.019.

Choi , S.U.S and Yu, W (2003) 'Journal of Nanoparticle Research, 2003, Volume 5, Number 1-2, Page 167'

Convery, N. and Gadegaard, N. (2019) '30 Years of Microfluidics', *Micro and Nano Engineering*, 2(November 2018), pp. 76–91. doi: 10.1016/j.mne.2019.01.003.

Das, S. K., Putra, N., Thiesen , P., and Roetzel, W. (July 17, 2003). "Temperature Dependence of Thermal Conductivity Enhancement for Nanofluids." ASME. *J. Heat Transfer*. August 2003; 125(4): 567–574.

Davis, B. (1942) 'Apparatus for Continuous Concentration of Solution under Reduced Pressure', *Industrial & Engineering Chemistry Analytical Edition*. American Chemical Society, 14(7), p. 548. doi: 10.1021/i560107a011.

Deb, K. *et al.* (2000) 'Reddy et al. 1999.pdf', pp. 849–858. doi: 10.1007/3-540-45356-3_83.

Deb, K. *et al.* (2002) 'A fast and elitist multi-objective genetic algorithm:NSGAII', 6(2), pp. 182–197.

Deb, K. *et al.* (2002) 'A fast and elitist multiobjective genetic algorithm: NSGA-II', *IEEE Transactions on Evolutionary Computation*, 6(2), pp. 182–197. doi: 10.1109/4235.996017.

Duangthongsuk, W. and Wongwises, S. (2017) 'An experimental investigation on the heat transfer and pressure drop characteristics of nanofluid flowing in microchannel heat sink with multiple zigzag flow

channel structures', *Experimental Thermal and Fluid Science*, 87, pp. 30–39. doi: 10.1016/j.expthermflusci.2017.04.013.

Eastman, J. A. *et al.* (2002) 'Anomalously increased effective thermal conductivities of ethylene glycol-based nanofluids containing copper nanoparticles', *Applied Physics Letters*, 78(6), pp. 718–720. doi: 10.1063/1.1341218.

Etaig, S., Hasan, R. and Perera, N. (2016) 'Investigation of a New Effective Viscosity Model for Nanofluids', *Procedia Engineering*. The Author(s), 157, pp. 404–413. doi: 10.1016/j.proeng.2016.08.383.

Fonseca, C. M. and Fleming, P. J. (1998) 'Multiobjective optimization and multiple constraint handling with evolutionary algorithms - Part I: A unified formulation', *IEEE Transactions on Systems, Man, and Cybernetics Part A:Systems and Humans.*, 28(1), pp. 26–37. doi: 10.1109/3468.650319.

Goel, T. (2007) 'Elitist Non-dominated Sorting Genetic Algorithm : NSGA-II Multi-objective optimization problem'.

Graham A.L.,(1981). On the viscosity of suspension of solid spheres, Appl. Sci. Res., 37 (3), 275-286

Hamilton, L and Crosser, O. K. , "Thermal Conductivity of Heterogeneous Two-Component Systems," Industrial & Engineering Chemistry Fundamentals, Vol. 1, No. 3, 1962, pp. 187-191. doi:10.1021/i160003a005

Hayat, T. *et al.* (2018) 'Flow of nanofluid by nonlinear stretching velocity', *Results in Physics*. The Author, 8, pp. 1104–1109. doi: 10.1016/j.rinp.2017.12.014.

Hosseini, M. S., Mohebbi, A. and Ghader, S. (2010) 'Correlation of Shear Viscosity of Nanofluids Using the Local Composition Theory', *Chinese Journal of Chemical Engineering*. Elsevier, 18(1), pp. 102–107. doi: 10.1016/S1004-9541(08)60329-8.

Jaluria, Y. *et al.* (2012) 'Heat transfer in nanofluids 2012', *Advances in Mechanical Engineering*, 2012. doi: 10.1155/2012/972973.Jamshidi, N. *et al.* (2012) 'Optimization of design parameters for nanofluids flowing inside helical coils', *International Communications in Heat and Mass Transfer*, 39(2), pp. 311–317. doi: 10.1016/j.icheatmasstransfer.2011.11.013.

Kalteh, M. (2013) 'Investigating the effect of various nanoparticle and base liquid types on the nanofluids heat and fluid flow in a microchannel', *Applied Mathematical Modelling*. Elsevier Inc., 37(18–19), pp. 8600–8609. doi: 10.1016/j.apm.2013.03.067.

Kamatchi, R. and Venkatachalapathy, S. (2015) 'Parametric study of pool boiling heat transfer with nanofluids for the enhancement of critical heat flux: A review', *International Journal of Thermal Sciences*, 87, pp. 228–240. doi: 10.1155/2012/435873.

Kaszynski, A. (2018) 'pyansys Documentation'.

Keblinski, P., Eastman, J. A. and Cahill, D. G. (2005) 'Nanofluids for thermal transport', *Materials Today*. Elsevier Ltd, 8(6), pp. 36–44. doi: 10.1016/s1369-7021(05)70936-6.

Koo, J. and Kleinstreurer, C "Viscous dissipation effects in microtubes and microchannels", International *Journal of Heat and Mass Transfer*, Vol.47, pp.3159–3169, 2004.

Krieger, I. M. and Dougherty, T. J. , "A Mechanism for Non-Newtonian Flow in Suspensions of Rigid Spheres," Journal of Rheology, Vol. 3, No. 1, 1959, pp. 137-145. doi:10.1122/1.548848

Kuerten, H. *et al.* (2011) 'Direct and large- eddy simulation VIII', *ERCOFTAC Series*, 15(April 2017). doi: 10.1007/978-94-007-2482-2.

Lauriat, G. *et al.* (2014) 'Heat Transfer in Nanofluids 2013', *Advances in Mechanical Engineering*, 6, p. 832415. doi: 10.1155/2014/832415.

Li, Z. *et al.* (2018) 'Energy transfer of Jeffery–Hamel nanofluid flow between non-parallel walls using Maxwell–Garnetts (MG) and Brinkman models', *Energy Reports*. Elsevier Ltd, 4, pp. 393–399. doi: 10.1016/j.egyr.2018.05.003.

Liang, Q. *et al.* (2017) 'Dispersion stability of thermal nanofluids', *Progress in Natural Science: Materials International*, 27(5), pp. 531–542. doi: 10.1016/j.pnsc.2017.08.010.

Lovison, A. *et al.* (2015) 'Parametrization of optimal trajectories for racing motorbikes Parametrization of optimal trajectories for racing motorbikes', (March).

Manay, E., Akyürek, E. F. and Sahin, B. (2018) 'Entropy generation of nanofluid flow in a microchannel heat sink', *Results in Physics*. The Authors, 9, pp. 615–624. doi: 10.1016/j.rinp.2018.03.013.

Masoumi, N. Sohrabi, N. A. BehzadmehrA new model for calculating the effective viscosity of nanofluids
J. Phys. D Appl. Phys., 42 (5) (2009), p. 55501

Mirzaei, M. and Dehghan, M. (2013) 'Investigation of flow and heat transfer of nanofluid in microchannel with variable property approach', *Heat and Mass Transfer/Waerme- und Stoffuebertragung*, 49(12), pp. 1803–1811. doi: 10.1007/s00231-013-1217-9.

Mukherjee, S. (2013) 'Preparation and Stability of Nanofluids-A Review', *IOSR Journal of Mechanical and Civil Engineering*, 9(2), pp. 63–69. doi: 10.9790/1684-0926369.

Nebbati, R. and Kadja, M. (2015) 'Study of Forced Convection of a Nanofluid Used as a Heat Carrier in a Microchannel Heat Sink', *Energy Procedia*. Elsevier B.V., 74, pp. 633–642. doi: 10.1016/j.egypro.2015.07.799.

Patel, P. D. and Russel, W. B. (1989) 'An experimental study of aqueous suspensions containing dissolved polymer: A. Phase separation', *Journal of Colloid and Interface Science*. Academic Press, 131(1), pp. 192–200. doi: 10.1016/0021-9797(89)90158-6.

Roache, P.J (1998). 'Verification and Validation in Computational Science and Engineering, Hermosa Publishers, Albuquerque,NM

Sajjad, M. *et al.* (2018) 'Numerical investigation of laminar convective heat transfer of graphene oxide/ethylene glycol-water nanofluids in a horizontal tube', *Engineering Science and Technology, an International Journal*. Karabuk University, 21(4), pp. 727–735. doi: 10.1016/j.jestch.2018.06.009.

Schaback, R. (2007) 'A practical guide to Radial Basis Functions', *Electronic Resource*, pp. 1–58.

Seppälä, A. *et al.* (2018) 'Correct interpretation of nanofluid convective heat transfer', *International Journal of Thermal Sciences*, 129(September 2017), pp. 504–531. doi: 10.1016/j.ijthermalsci.2017.11.003.

Sergis, A., Hardalupas, Y. and Barrett, T. R. (2018) 'Isothermal analysis of nanofluid flow inside HyperVapotrons using particle image velocimetry', *Experimental Thermal and Fluid Science*. Elsevier, 93(December 2017), pp. 32–44. doi: 10.1016/j.expthermflusci.2017.12.014.

Shah, Z. *et al.* (2018) 'Three dimensional third grade nanofluid flow in a rotating system between parallel plates with Brownian motion and thermophoresis effects', *Results in Physics*. Elsevier, 10(April), pp. 36–45. doi: 10.1016/j.rinp.2018.05.020.

Sigrist, J.-F. (2015) *Fluid-Structure Interaction*.

Singh, B. *et al.* (2016) 'Experimental and Numerical Analysis of Micro-Scale Heat Transfer using Carbon based Nanofluid in Microchannel for Enhanced Thermal Performance', *IOP Conference Series: Materials Science and Engineering*, 149(1). doi: 10.1088/1757-899X/149/1/012200.

Singh, B. *et al.* (2016) 'Experimental and Numerical Analysis of Micro-Scale Heat Transfer using Carbon based Nanofluid in Microchannel for Enhanced Thermal Performance', *IOP Conference Series: Materials Science and Engineering*, 149(1). doi: 10.1088/1757-899X/149/1/012200.

Sui, D., Langåker, V. H. and Yu, Z. (2017) 'Investigation of Thermophysical Properties of Nanofluids for Application in Geothermal Energy', *Energy Procedia*. The Author(s), 105(1876), pp. 5055–5060. doi: 10.1016/j.egypro.2017.03.1021.

Tjaden, B. *et al.* (2016) 'On the origin and application of the Bruggeman correlation for analysing transport phenomena in electrochemical systems', *Current Opinion in Chemical Engineering*. Elsevier, 12, pp. 44–51. doi: 10.1016/J.COCHE.2016.02.006.

Troschke, B. and Burkhardt, H. (1998) 'Thermal conductivity models for two-phase systems', *Physics and Chemistry of the Earth*, 23(3), pp. 351–355. doi: 10.1016/S0079-1946(98)00036-6.

Vanaki, S. M. *et al.* (2014) 'Effect of nanoparticle shapes on the heat transfer enhancement in a wavy channel with different phase shifts', *Journal of Molecular Liquids*. Elsevier B.V., 196, pp. 32–42. doi: 10.1016/j.molliq.2014.03.001.

Wang, X.-Q. Q. and Mujumdar, A. S. (2008) 'A review on nanofluids - part I: theoretical and numerical investigations', *Brazilian Journal of Chemical Engineering*, 25(4), pp. 613–630. doi: 10.1590/S0104-66322008000400001.

Xuan, Y. and Li, Q. (2000) 'Heat transfer enhancement of nanofluids', *International Journal of Heat and Fluid Flow*. Elsevier, 21(1), pp. 58–64. doi: 10.1016/S0142-727X(99)00067-3.

Xuan, Y., and Li, Q. (January 29, 2003). "Investigation on Convective Heat Transfer and Flow Features of Nanofluids." ASME. *J. Heat Transfer*. February 2003; 125(1): 151–155

Xue, Qingzhong & Xu, Wen-Mei. (2005). A model of thermal conductivity of nanofluids with interfacial shells. Materials Chemistry and Physics. 90. 298-301. 10.1016/j.matchemphys.2004.05.029.

Yang, Y. T., Wang, Y. H. and Huang, B. Y. (2015) 'Numerical optimization for nanofluid flow in microchannels using entropy generation minimization', *Numerical Heat Transfer; Part A: Applications*, 67(5), pp. 571–588. doi: 10.1080/10407782.2014.937282.

Yang, Y. T., Wang, Y. H. and Tseng, P. K. (2014) 'Numerical optimization of heat transfer enhancement in a wavy channel using nanofluids', *International Communications in Heat and Mass Transfer*. Elsevier B.V., 51, pp. 9–17. doi: 10.1016/j.icheatmasstransfer.2013.12.002.

Yu, W. & Choi, S. Journal of Nanoparticle Research (2003) 5: 167. https://doi.org/10.1023/A:1024438603801

Yu, F. *et al.* (2017) 'Dispersion stability of thermal nanofluids', *Progress in Natural Science: Materials International*, 27(5), pp. 531–542. doi: 10.1016/j.pnsc.2017.08.010.

Zitzler, E., Deb, K. and Thiele, L. (2000) 'Comparison of multiobjective evolutionary algorithms: empirical results.', *Evolutionary computation*, 8(2), pp. 173–195. doi: 10.1162/106365600568202.